City Research Online

City, University of London Institutional Repository

This is the accepted version of the paper.

This version of the publication may differ from the final published version.

Permanent repository link: https://openaccess.city.ac.uk/id/eprint/15460/

Link to published version: https://doi.org/10.1002/fld.4294

Turbulence Modelling and Role of Compressibility on Oil Spilling from a Damaged Double Hull Tank

Hao Yang[1], S. Yan[1,*], Q.W. Ma[1], Jinshu Lu[2], Yan Zhou[1]

1:School of Mathematics, Computer Science and Engineering, City University London, EC1V 0HB, London

2:Maritime College, Zhejiang Ocean University, Zhoushan, China, 316022

Abstract

The viscosity plays an important role and a multi-phase solver is necessary to numerically simulate the oil spilling from a damaged double hull tank (DHT). However, it is uncertain whether turbulence modelling is necessary, which turbulence model is suitable; and what the role of compressibility of the fluids is. This paper presents experimental and numerical investigations to address these issues for various cases representing different scenarios of the oil spilling, including grounding and collision. In the numerical investigations, various approaches to model the turbulence, including the large eddy simulation (LES), direct numerical simulation (DNS) and the Reynolds Average Navier-Stokes equation (RANS) with different turbulence models, are employed. Based on the investigations, it is suggested that the effective Reynolds numbers (Re) corresponding to both the oil outflow and the water inflow shall be considered when classifying the significance of the turbulence and selecting the appropriate turbulence models. This is confirmed by new lab tests considering the axial offset between the internal and the external holes on two hulls of the DHT. The investigations conclude for numerically simulating oil spilling from a damaged double hull tank (DHT) that when the effective Re is smaller the RANS approaches should not be used and LES modelling should be employed; while when the effective Re is large, the RANS models may be used as they can give similar results to LES in terms of the height of the mixture in the ballast tank and discharge but costing much less CPU time. The investigation on the role of the compressibility of the fluid reveals that the compressibility of the fluid may be considerable in a small temporal-spatial scale but plays an insignificant role on macroscopic process of the oil spilling.

Keywords: Turbulence modelling; compressibility; comparative study; oil Spilling; DHT

1. INTRODUCTION

Following the increase in oceanic energy exploration and transportation, the oil spilling from damaged oil pipelines or tankers, which poses a devastating impact on the marine environment, has become a significant global concern. Confronting the ship collisions and groundings, the double-hull tanker (DHT) technology was introduced in 1990s, and its effectiveness on reducing the global oil spillage has been demonstrated by relevant historical investigations [1-4]. However, the spilling incidents are still inevitable when ships suffering from structural damages, despite of great efforts devoted by the international communities. This calls for further studies on the mechanism of the oil

---

spilling from damaged hulls to guide the designs and operations of the DHTs for the purpose of reducing their potential risks to the marine environment.

When evaluating/investigating the oil spilling from damaged DHTs, the significance of the viscous effect is a fundamental issue. It was commonly assumed that the gravitational forces are much greater than the viscous forces and, therefore, the viscous effects can be ignored if the area of the interest is in the ultimate oil outflow from damaged DHTs. As a result, only the Froude similarity law was employed in early experimental studies, e.g. [5-7], and the viscous effects were ignored in the relevant analytical/empirical works (e.g. [7-12]) or numerical studies (e.g. [13]). Such simplification/assumption may not be acceptable if the dynamic process of the oil spilling is concerned. Generally speaking, when an oil tanker is subjected to a damaged condition due to collisions or groundings, the oil spilling affects the loads on the oil tanker and thus its motion, which mutually influence the behaviour of the spilled oil and eventually the ultimate oil outflow. This implies that the dynamic process of the oil spilling must be taken into account in order to accurately evaluate the oil outflow. For this purpose, the small-scale flow in the ballast tank between two hulls and/or near the broken holes, which shows significant viscous effects [13], must be investigated in detail. Although there are other uncertainties, ignoring the viscous effects in the similarity law may result in a severe scale effect in the time history of the oil outflow measured in the early experiment (e.g. [5]).

In more advanced studies, the viscous effects are commonly considered. In the relevant experimental works, e.g. [14-17], both the Froude and Reynolds scaling (the latter representing the viscous effects) were considered for both single hull oil tankers (SHTs) or DHTs. In analytical analysis based on steady or quasi-unsteady Bernoulli's equation (e.g., [18-21]), the viscous effects are taken into account through a discharge (viscous energy loss) coefficient. Recent numerical works are usually carried out by using multiphase Navier-Stokes models. For example, Tavakoli *et al* [18, 20] conducted two-dimensional (2D) numerical investigations to evaluate the oil spilling from grounded or collided DHTs with different hull designs, in which the finite volume method (FVM) is used, incorporating with the Volume of Fluid (VOF) to capture the interfaces between different phases; Yang *et al* [22] carried out a three-dimensional (3D) numerical simulation to explore the unsteady flow pattern associated with DHTs using a similar approach. In addition, there are also some numerical works on the oil spilling from SHTs, in which the numerical models or theories may be extended to the cases with DHTs. For example, Lu *et al* [15], Xiao *et al* [23], Krata *et al* [24] used VOF based FVM solvers; Koshizuka and Oka[25], Cheng *et al* [26] and Lee *et al* [27] adopted meshless methods based on the Moving Particle Semi-Implicit method (MPS).

However, in these numerical studies, the turbulence modelling is often ignored, partially due to its extra computing cost, which are not only spent on solving extra differential equations of turbulence models but also caused by the requirement of denser mesh resolutions and smaller time steps to resolve much smaller-scale turbulent behaviours. Only Lu *et al* [15], Yang *et al* [22] and Xiao *et al* [23] applied the *k-ε* model in their multiphase FVM solvers for the oil spilling from SHTs and demonstrated a promising agreement between the numerical results and the experimental data. The experiments in [15, 22] suggested that the spilling from a fixed SHT initially placed in still water is dominated by the oil outflow through the broken hole, which behaves similarly to a jet flow through

an orifice [22]; the Reynolds number (Re) of the oil outflow in the range of applications did not exceed 2000, falling in the laminar regime of the orifice flows (see, e.g. [28-30]), and the k-ε model may be sufficient.   In the cases with DHTs, the turbulence plays an important role in the ballast tank, as pointed out by Peter and Lin [13], although they did not consider turbulence modelling in their numerical simulation. More importantly, the features of the turbulence, particularly in the ballast tank of the DHTs, where both jet flows and free shear layers appear [22], are considerably different from that in the cases for SHTs. This means that implementing an appropriate turbulence model is more demanded in the cases with DHTs. Currently, it is not clear whether the k-ε model is suitable to deal with the cases with DHTs due to lack of guidelines targeting similar multiple-phase flow patterns in literature. Furthermore, it was found from our preliminary study [22] that, in the cases with DHTs, the time history of the recorded oil/water mixture in the ballast tank is sensitive to the types of the turbulence models; the k-ε model gave acceptable results in one case but wrong results in the other. Based on the knowledge available, the answers for the following questions are currently not clear: *(1) is it necessary to consider turbulence in numerical simulation of the oil spilling from DHTs, which requires extra computing cost?; and (2) if yes, which approach is the best to numerically model the turbulence in such cases?* It is worth noting that the large eddy simulation (LES, e.g. [31, 32]) and the direct numerical simulation (DNS, e.g. [33]) are generally known to be able to resolve the interfacial turbulence and the transition turbulence associated with free shear layers. Yang *et al* [22] has demonstrated the superiority of the LES over the Reynolds Average Navier-Stokes equation (RANS) approach with the k-ε model in one specific case. However, the LES or DNS require a much higher mesh resolution and much smaller time steps to achieve convergent results and, therefore, is more time-consuming, compared to the RANS approaches [34, 35]. Thus, the 'best' in Question (2) is in terms of the computational robustness and the questions may be interpreted as *how to select a turbulence modelling approach to give results with satisfactory accuracy but need less computational costs.*   To address this issue, it is essential to define a criterion in order to classify the range of the application of different approaches for turbulence modelling. Such criterion commonly depends on a purposely defined Reynolds number in literature. However, the Reynolds numbers used in the available numerical and experimental studies on the oil spilling from damaged DHTs and SHTs are all defined corresponding to the oil outflow, e.g. $\sqrt{g\Delta h_j}\Delta h_j/\gamma_{oil}$ employed in [13] where Δh_j and γ_{oil} are the ideal oil loss height evaluated by using the hydrostatic theory and the kinematic viscosity of the oil, respectively. It is not clear if such definition of the Reynolds number is suitable, considering the importance of the turbulence associated with the above-mentioned free-shear layers existing in the ballast tank of the DHTs.

Apart from these, our preliminary numerical study [22] has also identified sudden fluid-fluid or fluid-structure impacts associated with the jets of oil outflow and water inflow (either strikes on the walls of the ballast tank or the interaction between them occurs in the earlier stage of the spilling) and the entrapped air bubbles in the oil/water mixture in the ballast tank. Previous studies on water impact on structures, e.g. [36, 37], have identified the significant role of the compressibility of the fluids associated with the entrapped air bubbles and the violent impacts on structures in a very short duration of the impact. However, it is not clear so far (3) *how significant the effect of*

compressibility of the fluids on the oil spilling from DHTs, due to the fact that no existing numerical works in this field have considered the compressibility of the fluids to the best of our knowledge.

This paper aims to answer three questions indicated above, which are essential for efficiently modelling oil spilling from damaged DHTs. To do so, both the experimental and numerical investigations have been carried out. Various cases covering both the grounding and collision scenarios are considered. In the numerical aspect, various approaches, including the RANS approaches with different turbulence models, LES and DNS, are attempted in the comparative studies regarding the turbulence modelling; both the incompressible solver and the compressible solver are adopted to identify the role of the compressibility in these cases. We assume that the chemical reactions, e.g. oil-water emulsion, and the thermodynamics are ignored in the numerical simulation.
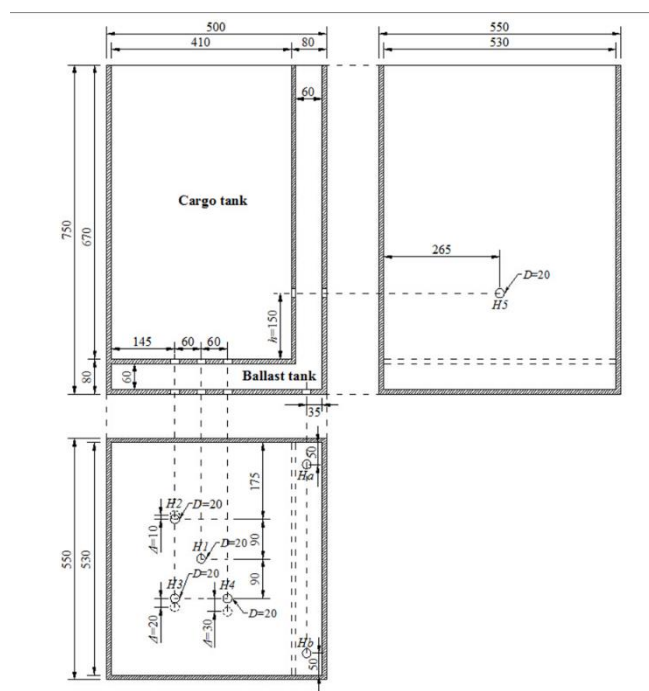

Figure 1 Model tank and configuration of the holes(unit: mm, solid circles: holes on the cargo tank; dashed circles: holes on the external tank)
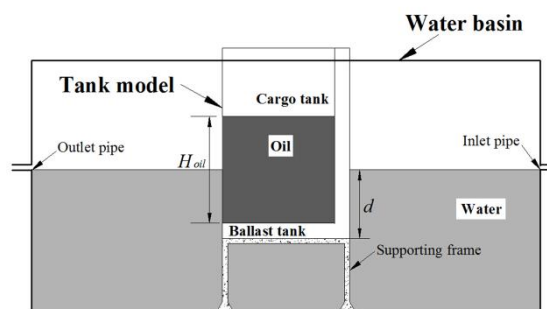

Figure 2 Sketch of the water basin and the DHT model

2. EXPERIMENTAL AND NUMERICAL CONFIGURATION

The experimental investigations are carried out at the Zhejiang Ocean University, China. A model tank is built at 1/40 scale of a typical cargo tank section of VLCC ([5, 38]) but ignoring the details

of the internal support structures inside the ballast tank. Similar to the work done in [5], a J-shape double hull configuration (sketched in Fig.1) is used. The height, breadth and length of the external hull are 0.75m, 0.5m and 0.55m respectively. The model is made of watertight plywood and glass for visual observations. The height of the bottom ballast tank (h_b) and the width of the side ballast tank (w_s) are all 6cm. Due to the limitation in the material, the thickness of the glass wall (t_g) does not follow the exact geometric similarity but is taken as 1cm. Both the Froude and Reynolds similarity are adopted to achieve the kinematic and dynamic similarities following the work done in [17]. Based on the Reynolds similarity, the canola oil with density of 915 kg/m^3 and viscosity of 3.2×10^{-5} m^2/s is chosen as the oil in model tests. This corresponds to the industrial extra heavy crude oil in the real situation, i.e. the dynamic viscosity of extra heavy crude oil ranges 1.5-5Pa·s with the density larger than 932kg/m^3 ([17, 39]). The density and the kinematic viscosity of water are 998 kg/m^3 and 10^{-6} m^2/s, respectively. For simplification, the DHT model tank is fixed in a water basin as illustrated in Fig.2. The water in the water basin is initially at rest. Inlet and outlet pipes are connected to the water basin to ensure a constant draft of the DHT (d) of 27cm during the experiment.

The oil spills from the model tank through smooth-edged circular punctures with diameter of D, which are drilled into the tank bottom plates or side plates, as illustrated in Fig. 1. For each case, one hole on the external hull (referred to as the external hole and marked by dashed circles in Fig.1) and one on the internal hull (referred to as the internal hole and marked by solid circles in Fig. 1) are open simultaneously and the others remain closed. Following the previous works, the grounding scenario is simplified as the oil spilling from a group of holes on the bottom plates, whereas the spilling from a group of holes on the side plates is considered as a simplified collision scenario. In the existing experimental and numerical studies, these groups of holes are mainly configured to be coaxial and orthogonal to the hull surface, e.g. [16]. In this study, different axial offsets (Δ) between the centres of the internal and external holes are considered. Compared to the existing coaxial configuration, the consideration of the axial offset widens the range of the application, bringing the experiment a step further to the reality. The cases to be considered in this paper are summarised in Table 1, although more have been done in the experiment.

Table 1 Summary of the test cases

Case No.	Scenarios	Spilling hole group	Initial height of oil (cm)	axial offsets Δ (cm)
C1	Collision	H5	38	0
G1	Grounding	H1	42	0
G2	Grounding	H2	42	1
G3	Grounding	H3	42	2

Note: The diameters of the holes (D) are all 2cm, the drafts of the DHT (d) are all 27cm.

The test is carried out in a controlled environment with temperature of $10\pm3℃$. PTP703 level sensors are used to measure the mean level of the oil surface in the cargo tank and that of the oil/water mixture in the ballast tank. The sensitivity and the accuracy of the sensors have been initially tested to ensure an accurate reading. For the purpose of comparison, metric rulers (accuracy at 1mm) attached to different locations of the DHTs are also used to manually record the

surface elevations. During the experiment, the oil spilling launches as one chosen group of holes are opened instantaneously. The time histories of the level of water/oil mixture in the ballast tank, $H_{mixture}$ (measured from the bottom of the ballast tank), and the height of the oil in the cargo tank, H_{oil}, are recorded. The spilling processes are recorded by two HD camcorders. Tests on all cases have been repeated and the mean differences in term of the time history of the measured data are within 1%.

The numerical investigations are carried out by using OpenFOAM, which is the open-source computational fluid dynamics (CFD) software. Both the incompressible and compressible Navier-Stokes equations with the Newtonian fluid assumption are used to describe the conservation of the mass and momentum. The governing equations are solved by using FVM with the VOF method to capture the interface between two immiscible phases. The fluid density and viscosity in the momentum equation and the continuity equations are substituted with weighted average values of those of air, water and oil, depending on their corresponding volume fractions. The solver implements the robust transient PIMPLE (merged PISO-SIMPLE) algorithm for the pressure-velocity coupling. Readers may be referred to [40] for more details. The surface tension effect is considered in the numerical investigation through the Continuum Surface Force (CSF) method with typical surface tension coefficients of the model-test fluid, i.e., $\sigma_{air-oil}$=0.032N/m ([41]); $\sigma_{air-water}$=0.072N/m ([42]); $\sigma_{oil-water}$=0.002N/m ([43]). It should be noted that the VOF models may not reflect the nonlinear behaviour of the viscosity associated with the emulsified oil ([44]) due to their inherent limitation that the viscosity of the mixture varies linearly following the volumes of the fraction of the fluids. To avoid this issue, we only present the cases where the oil emulsion is insignificant in the corresponding studies.

In order to answer Question (1) and (2) listed in the Introduction, different approaches to resolve the turbulence, including the RANS with different turbulence models, LES and DNS, are considered in the investigation. As indicated above, the LES is widely accepted for modelling the free surface flows and jet flows (e.g. [31, 32]). Nevertheless, it has not yet been attempted in the problems addressed in this paper. Here the LES with the one-equation sub-grid eddy viscosity model will be utilized for simulating the oil spilling through damaged DHTs. This model accounts for the sub-grid scaling stress using a Boussinesq type assumption ([45-47]) to capture the small-scale eddies, which are isotropic in nature. The reason for why choosing this one rather than others are due to two folds. One is that the model has been examined in a wide range of turbulent problems and shows a superiority over the Smagorinsk's eddy viscosity model especially if the flow is highly complex and has shear flows as described by [45, 48], which has also been confirmed in our preliminary studies. Furthermore, the errors of this model in terms of experimental data are lower than 5% for all cases considered in this paper. This can be considered to be acceptable. The second reason is that the main purpose of this study, i.e. selecting a suitable turbulence modelling approach to satisfy a satisfactory accuracy with less computational time and the purpose can be achieved by using the one equation LES model, with other LES models, e.g. the dynamic eddy viscosity model, the dynamic sub-grid kinetic energy model and the stochastic backscatter model [48], to be tested in the future work. The RANS uses time-averaged Navier-Stokes (NS) equations, through which the unsteady flow-field is ensemble-averaged, and the effects of turbulence are represented by the Reynolds stress tensor, which is usually solved by using appropriate turbulence models, such as the

well-known *k-ε* and *k-ω* models. The RANS approaches generally require shorter CPU time to get convergent results, however, the question is *under which condition, the RANS approaches may lead to satisfactory solutions for the oil spilling from DHTs (Question 2), because they are known to be tuned and calibrated for specific flow features excluding the situations concerned with DHTs. Therefore, various RANS approaches, including the standard *k-ε*, RNG *k-ε,* Launder-Sharma low-Re *k-ε,* realizable *k-ε* and *k- ω* SST models, are employed in this paper. Compared to the LES and the RANS approaches, the DNS requires much denser mesh to get a convergent solution but can fully resolve the turbulence. This means that by using the same computational mesh as the one required by the LES, the results of the DNS may be under resolved. Therefore, this does not fit our main objective on seeking an efficient turbulence modelling. Nevertheless, one may agree that for a specific mesh resolution, the difference between the result of the under-resolved DNS and that of the LES may reflect the overall effect of the sub-grid stress. Considering this, an under-resolved DNS is also employed in this investigation to shed some light on the significances of the sub-grid stress in the LES.
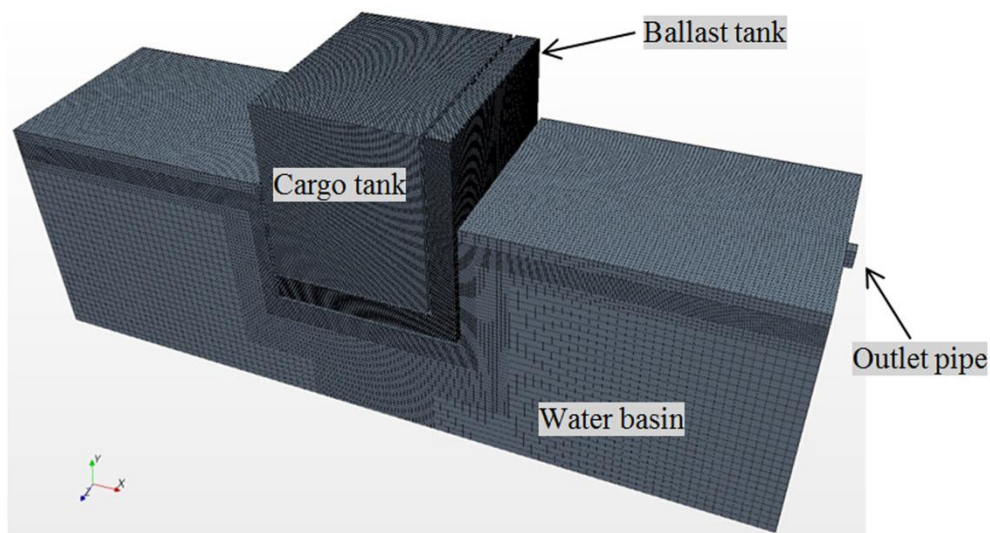
(a) Computational domain and mesh
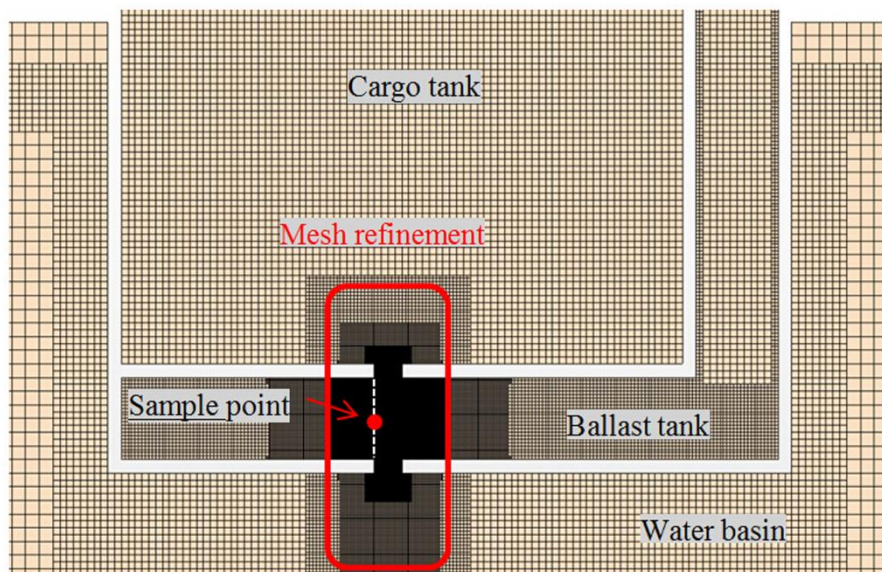
(b) Illustration of the spatially hierarchical mesh refinement
Figure 3 Sketch of the computational domain and mesh

A computational domain consistent with the experimental configuration is adopted. The heights of the air layers above the water surface in the water basin and the oil surface in the cargo tank are determined based on numerical tests to ensure the boundary on the top of the computational domain does not affect the numerical results. On the walls of the water basin and the DHT, a non-slip boundary condition is employed and an appreciated wall function is chosen for the turbulence models. On the top boundary, a pressure outlet condition is imposed. The computational mesh is hexahedral, as illustrated in Fig. 3(a). A reference mesh size of 2cm is used, which represents the maximum mesh size in the computational domain. Broadly speaking, the mesh size shall be sufficiently small near the holes ([49]); it shall be also sufficient to resolve the interface between different phases and minimise the numerical diffusion ([50]). A spatially hierarchical mesh refinement is adopted in such areas to provide sufficient mesh resolutions. One example is displayed in Fig.3(b) for demonstration. By using the spatially hierarchical refinement, the ratio (α_{ds}) of the minimum cell size to the maximum mesh size may be used to reflect the overall mesh resolution in the convergence investigation. More detailed description of the mesh refinement can be found in [22].

It may be worth noting the novelty and the necessity of adopting the cases, where the internal and the external holes are not coaxial, in the current study. As indicated in the Introduction, the Reynolds number commonly defined in the existing studies on the oil spilling from damaged DHTs commonly corresponds to the oil outflow (e.g. [13]). Nevertheless, limited tests in our previous study [22] have revealed that both the oil outflow and the water inflow may be significant in the ballast tank and behave as convective shearing layers. This means that the effects of the water inflow must also be considered in order to classify the significance of the turbulence in the ballast tank and to select a robust approach for turbulence modelling. In the Cases G1, G2 and G3, the hydrostatic condition (the draft of the DHT and the initial height of the oil in the cargo tank) are the same, leading to the same ideal oil loss height evaluated by using the hydrostatic theory and the same Reynolds number of the oil outflow as defined in [13]; however, different axial offsets lead to different patterns of the shearing flows, particular the oil outflow and the water inflow, in the ballast tank. The corresponding investigations on these cases especially contribute to Question 2 for the purpose of finding a suitable criterion to guide the selection of an appropriate turbulence model for efficiently modelling the oil spilling from DHTs. It is noted that the significance of the water inflow may also be changed through changing the initial oil heights in the cargo tank or the initial draft of the DHT using coaxial configurations. Nevertheless, in such a way, the Reynolds number corresponding to the oil outflow varies consequently, leading to inconvenience on discussing the effects of the water inflow on Questions 1 and 2.

It is also noted that, for all cases considered in the numerical investigations, convergence tests are carried out a prior for the LES and the RANS approaches. Considering the fact that a self-adopted time step satisfying the Courant condition (i.e., Courant number $C_o < 0.5$), which links the convergence and stability properties associated with the time step size to the mesh size ([51]), is applied in the numerical simulation, only the convergence property against the mesh size is required in the tests. Different mesh resolutions, specified by using α_{ds}, are used. In order to save the space, only corresponding results for one case are presented here for demonstration. In this case, the oil

spills from one set of coaxial bottom punctures (axial offsets $\Delta = 0$, marked by 'H1' in Fig. 2) with D =2 cm. The initial H_{oil} is set as 42cm and the draft of the tank d is kept as a constant value of 27cm. This case is referred to as 'Case G1' in Table 1 and represents a simplified grounding scenario, similar to the work done in [7, 13, 17]. In the convergence tests, the value of α_{ds} ranges from 1.5625% to 6.25%, yielding that the number of the cells per diameter of the holes in horizontal direction varies from 64 to 16 and the number of cells along the vertical axis through the centres of the holes ranging 224~56; the total number of cells varies from approximately 4 to 0.7 million.
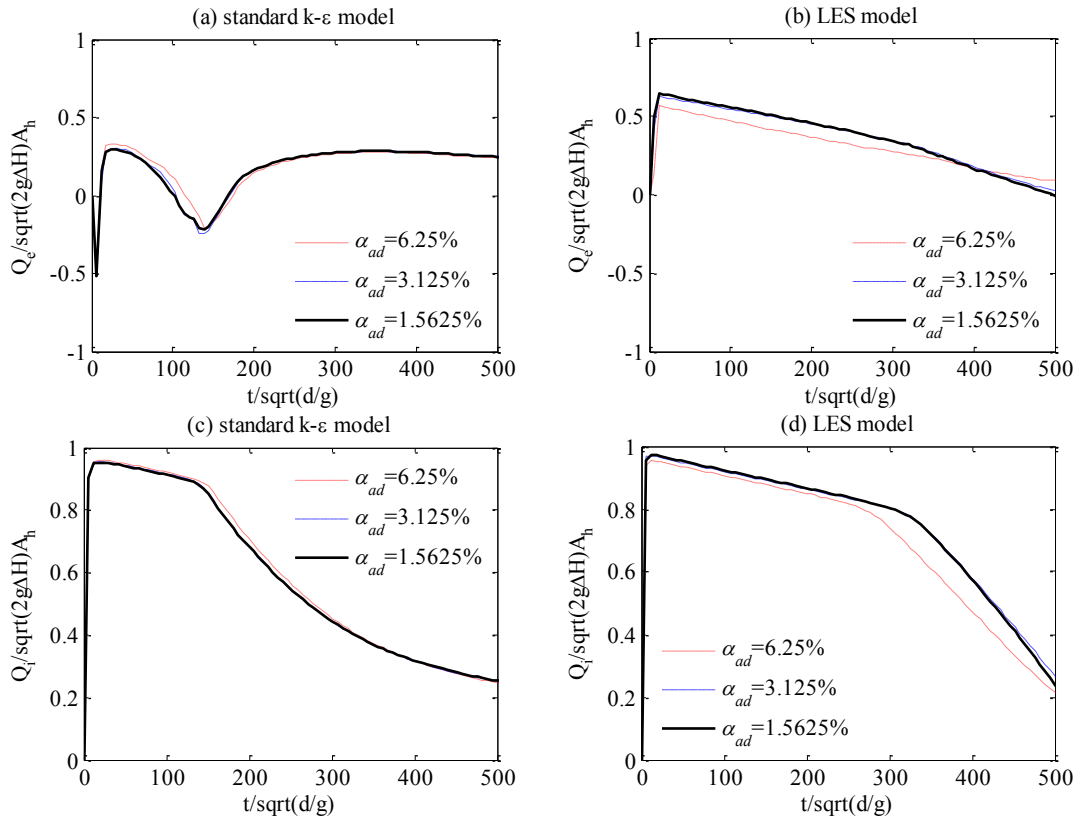

Figure 4 The time histories of the volumetric flow rate through the internal (Q_i) and external hole (Q_e) in the cases with different mesh sizes (Case G1, D =2 cm, $\Delta = 0$, $d = 27$cm, initial $H_{oil} = 42$cm)
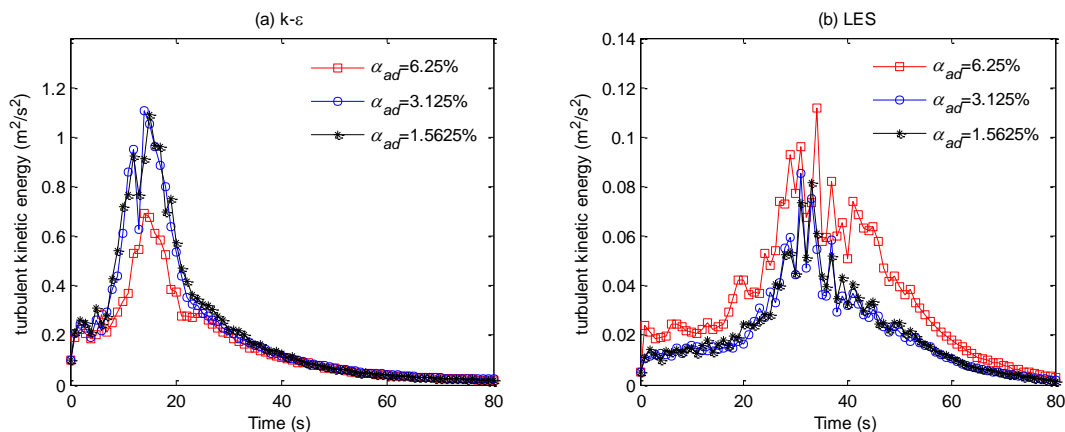

Figure 5 Time histories of the turbulent kinetic energy at the sample point (Fig 3b) in the cases with different mesh sizes (Case G1, D =2 cm, $\Delta = 0$, $d = 27$cm, initial $H_{oil} = 42$cm)

Fig. 4 illustrates the time histories of the discharge of the oil/water mixture through the external hole, Q_e (a positive value indicates an outflow from the ballast tank towards the external water), and

the internal hole, Q_i (a positive value indicates an outflow from the cargo tank towards the ballast tank), in the cases with different mesh sizes and different approaches for turbulence modelling. For convenience, the time and the discharge are nondimensionlised by using $\sqrt{d/g}$ and $\sqrt{2g\Delta H}A_h$, respectively, where ΔH is the initial elevation difference between the oil surface in the cargo tank and the external water level. It is observed that for both the LES and the k-ε model, the results with α_{ds}=3.125% agree well with those using a finer mesh, i.e. α_{ds}=1.5625% but are visually different from those using a coarser mesh, i.e. α_{ds}=6.25%. Considering the fact that the discharge indicates a spatially averaged velocity through the holes and may not represent the feature of the turbulent flow in a smaller scale, other turbulence-related parameters, e.g. the turbulent kinetic energy, is also examined at some specific locations of interest. These include the locations inside the boundary layers attached to the solid wall near the holes and near the interfaces between different phases, where the turbulence is expected to be either more significant or more sensitive to achieve correct results ([31]). Fig. 5 compares the turbulent kinetic energy in the cases with different mesh sizes at the midpoint between left bottom corner of the internal hole and the left top corner of the external hole on the central vertical plane (as illustrated in Fig. 3(b)), which is mainly located on the interfacial region between oil and air phases in the ballast tank before it becomes submerged. For clarity, corresponding results with a time interval of 1s are plotted in Fig.5, although the actual time step size used in the numerical simulation is at the level of ~10^{-4}s. A similar convergence property can be observed. The time averaged relative differences, which is defined in the same way as [52], of turbulent kinetic energy between α_{ds}=3.125% and α_{ds}=1.5625% shown in Fig. 5(a) and (b) are approximately 1.4% and 1.6%, respectively, which can be considered as acceptable.

3. COMPARATIVE STUDY ON TURBULENCE MODELS

One may find from Figs. 4-5 that different turbulence models lead to significantly different results. A systematic investigation is carried out in order to address Questions 1-2 listed in the Introduction related to the turbulence models. In the numerical investigation presented in this section, the compressibility of the fluids is ignored and the incompressible flow solver is applied. The role of the compressibility will be discussed in Section 4.

Our experiments on oil spilling from a fixed DHT in still water have revealed two common physical processes closely associated with the significance of the turbulence. The first one occurs during oil/water mixture passing through the damaged holes on the DHTs, which may behave similar to jet flows through an orifice (Figs. 13, 17 or [22]). The second one takes place near the interface between different phases, e.g. the oil/water/air interface inside the ballast tank, where the transition turbulence triggered by the free-shear layers may play important role. As observed in our experiment (Fig. 18 or [22]), the oil jet spilled from the cargo tank may behave violently and therefore the oil/air interface may be broken. In order to identify an appropriate approach to efficiently model the turbulence associated with the oil spilling from the DHTs, the LES-based one equation eddy viscosity model (refer to as the LES model), RANS with the standard k-ε model, RNG k-ε, realizable k-ε, Launder-Sharma low-Re k-ε and k-ω SST models, and the DNS are employed for this purpose. Considering the limit of the laboratory model tests on measuring micro-scale flow fields, two macroscopic parameters, i.e. H_{oil} and $H_{mixture}$, are examined. For the

case with DNS, the mesh sizes used are the same as the one used by LES according to relevant convergent investigation, although the mesh resolution required by the DNS may be under-resolved.
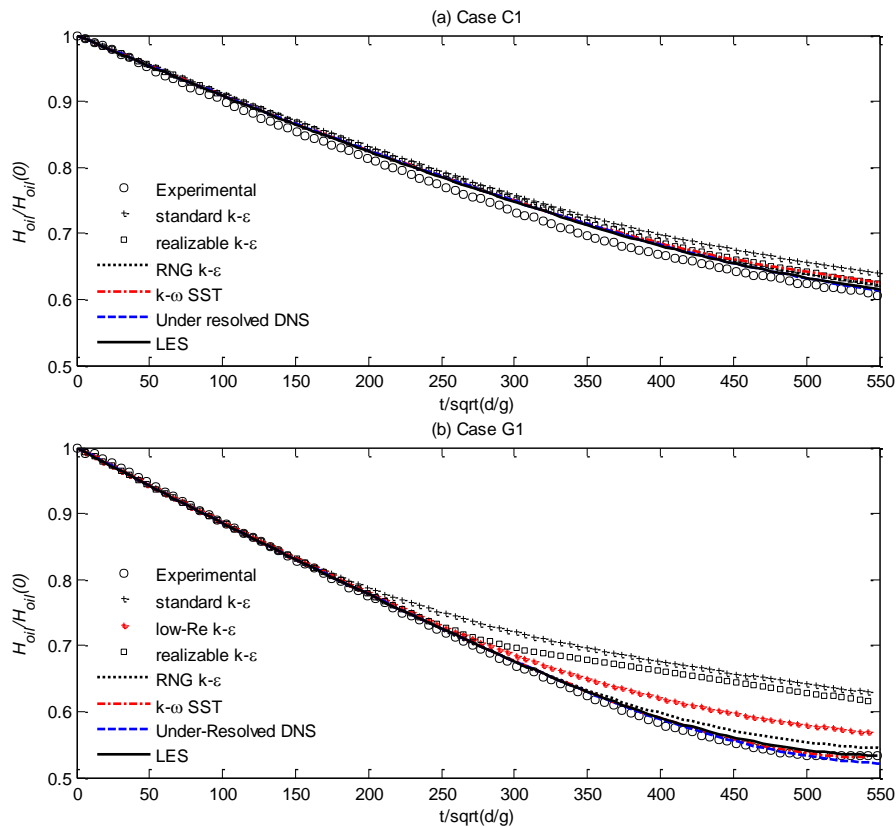

Figure 6 Time histories of the oil height in the cargo tank (H_{oil}) in the cases with different turbulence modelling (Case C1: D =2 cm, Δ = 0, d = 27cm, initial H_{oil} = 38cm; Case G1, D =2 cm, Δ = 0, d = 27cm, initial H_{oil} = 42cm)

The height of the oil left in the cargo tank (H_{oil}), reflecting the discharge through the internal hole, is firstly considered. The time histories of H_{oil} in the cases with different turbulence modelling approaches are plotted in Fig.6. In addition to the results from Case G1 (representing a simplified grounding scenario) introduced in Section 2, those from another case representing a simplified collision scenario, i.e. Case C1, are also plotted. In Case C1, a set of coaxial punctures on the side wall (marked as H5 in Fig.2) are regarded as the spilling hole and the initial value H_{oil} is 38cm. All other conditions are the same as Case G1. Similar to Fig. 5, the time and H_{oil} are nondimensionlised by $\sqrt{d/g}$ and the initial value of H_{oil} (denoted by $H_{oil}(0)$), respectively. As observed from this figure, all numerical results agree well with the experimental data in Case C1 (Fig. 6(a)) no matter which turbulence modelling approaches are used. However, in Case G1(Fig.6(b)), most of the approaches lead to a satisfactory agreement with the experimental data, except the standard, realizable and low-Re k-ε models, whose results seem to diverse from others at the dimensionless time larger than approximately 160, 240 and 250 respectively. At $t\sqrt{g/d} \approx 160$, the internal hole becomes fully submerged in the case using the standard k-ε model but not in other cases as shown in Fig.7(b). It is understandable that the hydrostatic features or the potential head difference dominating the flow through the internal hole (thus the change of H_{oil}) are different before and after such instant, as discussed in [22]. This may directly explain the diversion of the time history of H_{oil} at $t\sqrt{g/d} \approx 160$ between the standard k-ε model and others. Similar mechanism can be used to

explain the diversion of the result by the realizable k-ε model or the low-Re k-ε model and the experimental results at $t\sqrt{g/d} \approx 240$ or 250, which corresponds to a similar instant in the case using the realizable k-ε model or low-Re k-ε model, respectively. This implies that the height of the oil in the cargo tank during spilling may be considerably affected by the characteristics of the flow in the ballast tank, which will be discussed below. This also suggests that the conclusion about the turbulent effects on the height of the oil left in the cargo tank drawn based on the investigations of the oil spilling from SHTs, for example, Lu *et al* [15], Xiao *et al* [23] and Yang *et al* [22] claiming that the k-ε models lead to promising accuracy for predicting the oil spilling from SHTs, may not be extended to the problems associated with DHTs.
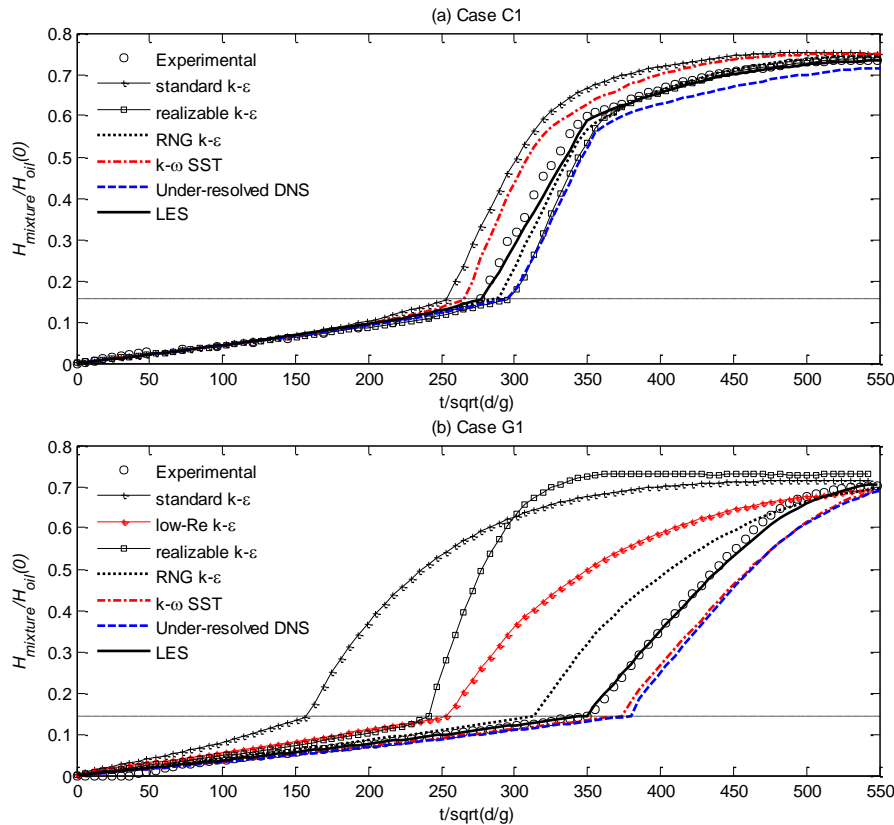

Figure 7 Time histories of the height of the mixture in the ballast tank ($H_{mixture}$) in the cases with different turbulence models (Case C1: D =2 cm, $\varDelta$ = 0, d = 27cm, initial H_{oil} = 38cm; Case G1, D =2 cm, $\varDelta$ = 0, d = 27cm, initial H_{oil} = 42cm; the horizontal dash-dotted line refers to the height of the bottom ballast space)

The height of the oil/water mixture in the ballast tank ($H_{mixture}$), which is determined by the discharges through both the internal and external holes, is also examined. The time histories obtained by using different turbulence modelling approaches and measured in the laboratory are presented in Fig. 7. From this figure, one may find that the time history of $H_{mixture}$ in both cases has a sudden transition when $H_{mixture}$ reaches the level represented by a horizontal dash-dotted line, referring to the height of the bottom ballast space (h_b). This is caused by a sudden change of the horizontal cross-sectional area of the ballast tank at this position (see Fig. 1 for details). For clarity, the corresponding results of the volumes of the oil/water mixture ($V_{mixture}$) in the ballast tank are illustrated in Fig. 8, in which $V_{mixture}$ is nondimensionlised by V_b, the volume of the ballast tank. From Figs. 7-8, it is observed that the numerical results are sensitive to different turbulence

modelling approaches. In both cases, the standard k-ε model results in a much quicker increase of the mixture in the ballast tank, whereas the under-resolved DNS underestimates the rate of the increment of the mixture. It is also interesting to find that the realizable k-ε model, RNG k-ε model and k-ω SST model do not only produce values of $H_{mixture}$ or $V_{mixture}$ considerably different from the experimental data, but also show different trends of error in different cases. For example, the k-ω SST model overestimates the rate of the increase of the mixture level in Case C1 but underestimate that in Case G1. This implies uncertainties in estimating the errors caused by these models. The low-Re k-ε model seems to produce a better result compared to the realizable k-ε model, as observed from Fig. 6(b), 7(b) and 8(b), which shows that the results by the low-Re k-ε model is close to that by the realizable k-ε model before $t\sqrt{g/d} \approx 240$ and then shifts towards that by the RNG k-ε model. If one would have followed the suggestions by, for example, [15, 22, 23], and use the k-ε models to model the cases for the DHTs, one would obtain wrong results for the height of the oil/water mixture in the ballast tank.
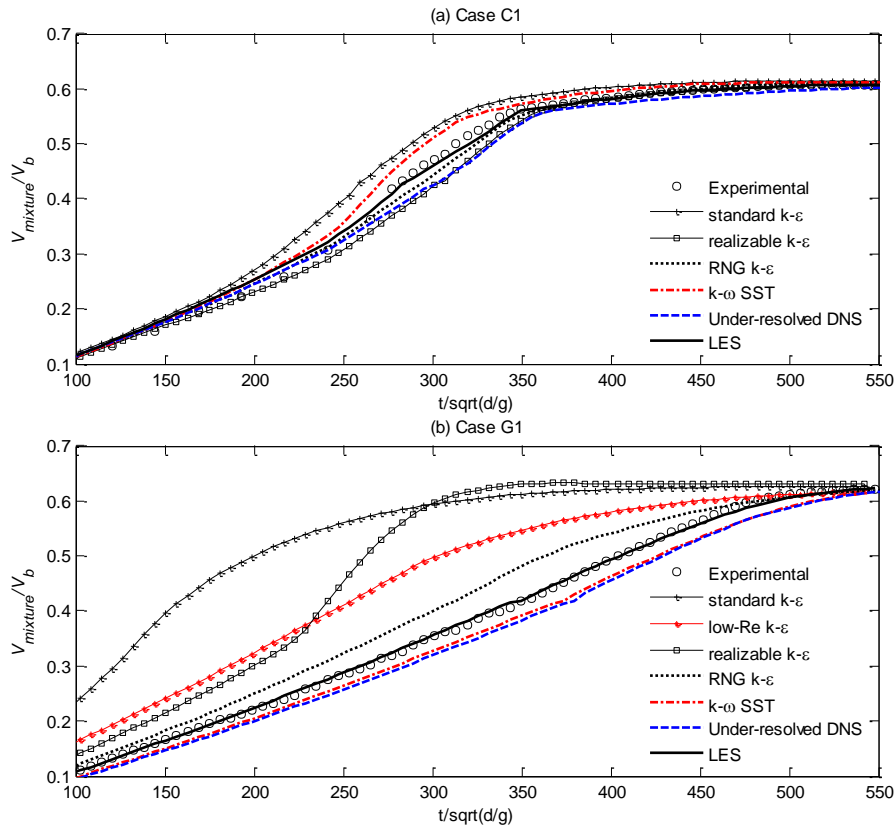

Figure 8 Time histories of the volume of the mixture in the ballast tank ($V_{mixture}$) in the cases with different turbulence models (Case C1: D =2 cm, Δ = 0, d = 27cm, initial H_{oil} = 38cm; Case G1, D =2 cm, Δ = 0, d = 27cm, initial H_{oil} = 42cm)

Furthermore, it has been found that the results of the under-resolved DNS agree well with the experimental data in terms of H_{oil} (Fig.6). However, Fig 7 shows that the corresponding results for $H_{mixture}$ are considerably different from the experimental data. This is due to the different characteristics of the flows influencing them. H_{oil} corresponds to the oil discharge through the internal hole and is dominated by the oil motion inside the cargo tank, which behaves similarly to an orifice, and driven mainly by the gravity. The Reynolds numbers (R_e) with the length scale specified by the diameter of the hole for oil outflow through the internal hole are approximately

1200 and 1800 in Case C1 and Case G1, respectively, implying a laminar regime (for orifice flow, the upper limit of R_e for the laminar regime is 2000, as suggested by [28-30]). In this area, the turbulence, especially the effects of the sub-grid stress or the extra turbulence viscosity, is not significant. The DNS model with the present mesh resolution may be sufficient. However, $H_{mixture}$ reflects an overall effect of the flows through the internal/external holes and the motion of fluids in the ballast tank, which shows complex features of multiple phase flows and may involve violent fluid impacts, broken interfaces between different phases and entrapped air bubbles. The turbulence plays a more important role. The present under-resolved model fails to properly model the associated turbulence to achieve satisfactory results in the ballast tank, suggesting a significant effect of the sub-grid stress.
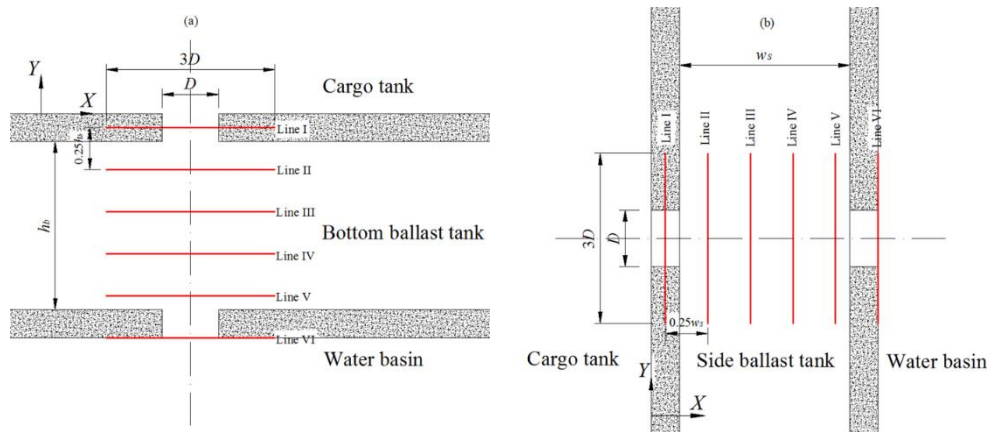

Figure 9 Sketch of the sampling lines at the central vertical plane near the holes for Case G1 (a) and Case C1 (b)

It is worthy of noting that all numerical results displayed in Figs. 6-8 are convergent, except the under-resolved DNS, as demonstrated in Section 2 and the differences are caused by different turbulence modelling approaches. As expected, the LES leads to the most accurate results, which agree well with the experimental data for both macroscopic parameters (H_{oil} and $H_{mixture}$) in both cases. The relevant results from the LES modelling are considered as correct solutions for further comparisons on the kinematic and dynamic characteristics of the flow inside the ballast tank, due to the lack of experimental data on these parameters. Such comparison aims to shed some light on why different turbulence models lead to significantly different results in Figs.7-8. To do so, some sampling lines at different cross-section between holes on internal and external hulls in Case G1 and Case C1 are introduced as shown in Fig. 9. Relevant distributions of the parameters have been compared. We firstly focus on Case G1, where the corresponding results are more sensitive to the selection of the turbulence modelling(Fig. 6(b) and 7(b)).

Fig. 10 shows the velocity head ($V^2/2g$) and the pressure distributed at different sampling lines at $t\sqrt{g/d} \approx 12$ in Case G1. For convenience, they are normalised by using $H_{oil}(0)$ and the atmospheric pressure (P_{atm}). As observed from Fig.10, near the internal hole (Line I), the velocity head and the pressure predicted by using different turbulence modelling approaches are close to each other. However, as the location of the observation moves further towards the external hole, more significant difference can be observed. This suggests a considerable underestimation of the outflow

through the external hole, due to the overestimation of the turbulent energy loss by the standard and realizable k-ε models.
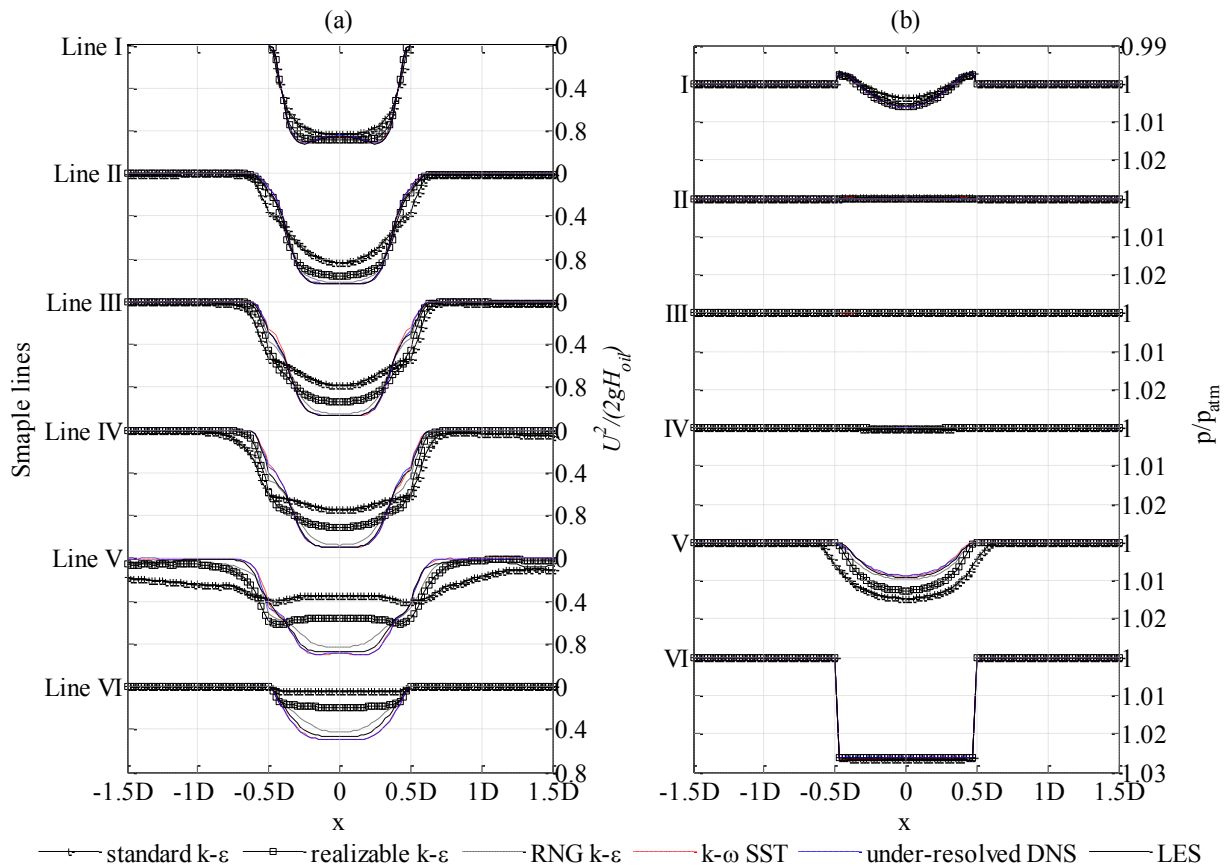

Figure 10 Distribution of (a) the velocity head and (b) the normalized pressure (p/P_{atm}) along the horizontal sampling lines at $t\sqrt{g/d} \approx 12$ in the cases with different turbulence modelling in Case G1 (D = 2 cm, Δ = 0, d = 27cm, initial H_{oil} = 42cm)

It is clearer in Fig. 11 which illustrates the turbulent kinetic energies in the region near the broken holes obtained by using different turbulence modelling. From Fig.11, a significantly higher level of the turbulent kinetic energy is observed in the main body of the oil jet given by the standard, low-Re and realizable k-ε models. A similar conclusion has also been made in the comparative studies associated with the orifice flow, suggesting that the standard and realizable k-ε models may yield undesirable results for the cases with Reynolds numbers similar to the Case G1, i.e. Re<2000 (e.g., [53, 54]). The low-Re k-ε model performs better than the realizable k-ε models, partially attributing to the empirical treatment of the flow near the wall with local low turbulent Reynolds number effects and the wall damping effects [55,56]. Compared to the standard, low-Re and realizable k-ε models, the RNG k-ε model shows a dramatic improvement, perhaps attributing to its special concern on smaller scales of the fluid motion, making it more feasible to deal with the turbulence associated with the interface between different phases and triggered by convective shearing layers . Our conclusion on the poor performance of the k-ε models also conforms to the comments by [57], i.e. without special treatment of a turbulence damping, the differential eddy viscosity models, such as the k-ε models, generate levels of turbulence that are too high throughout the interface of the multi-phase flow. It is also found from Fig. 10(a) that the k-ω SST model leads to a better estimation of the velocity head (and turbulent energy loss) compared to the k-ε models, conforming

to existing conclusion on the suitability of the k-ω SST model on dealing with a Low-Re problems without any extra damping functions ([58, 59]).
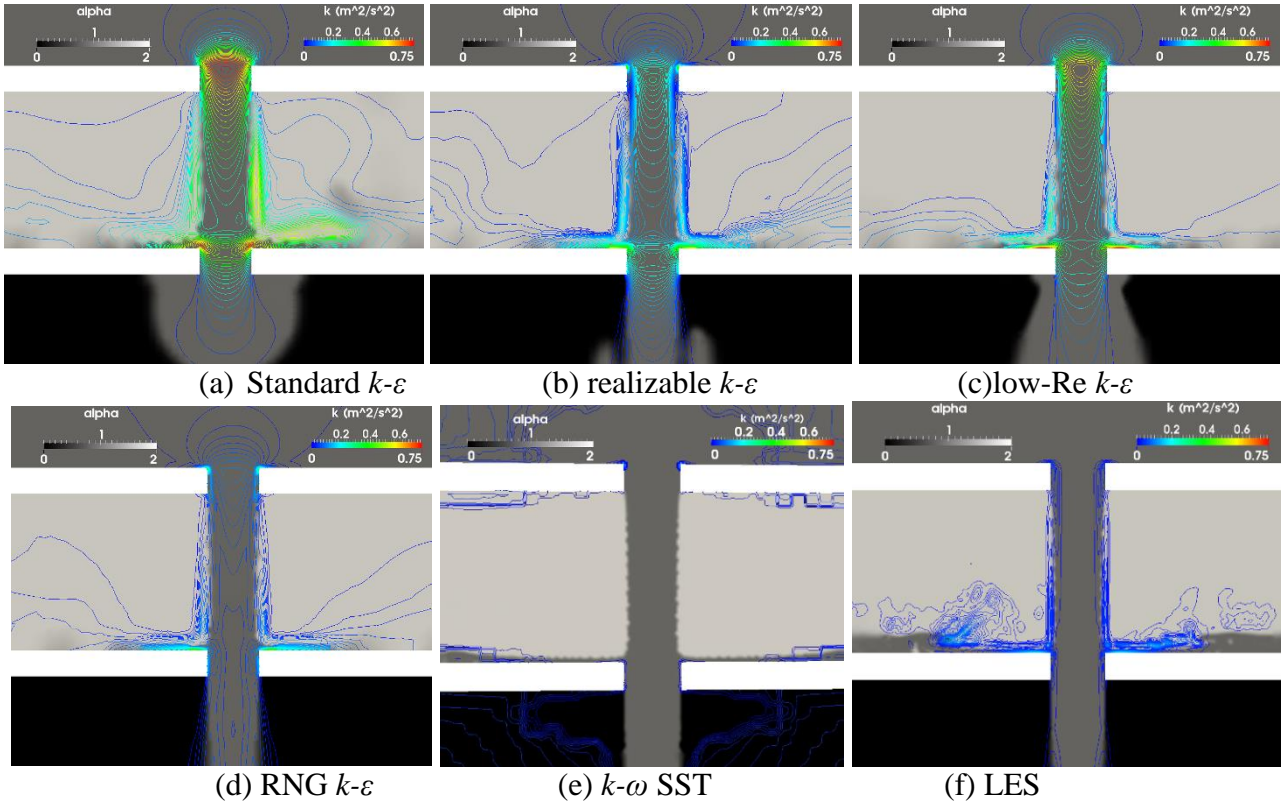

(a) Standard k-ε (b) realizable k-ε (c) low-Re k-ε

(d) RNG k-ε (e) k-ω SST   (f) LES

Figure 11 Spatial variation of the turbulent kinetic energy (k) at $t\sqrt{g/d} \approx 12$ in Case G1 using RANS with different turbulence modelling (D = 2 cm, $\varDelta$ = 0, d = 27cm, initial H_{oil} = 42cm; the volume fraction, i.e. alpha, are 0, 1 and 2 for water, oil and air phase)
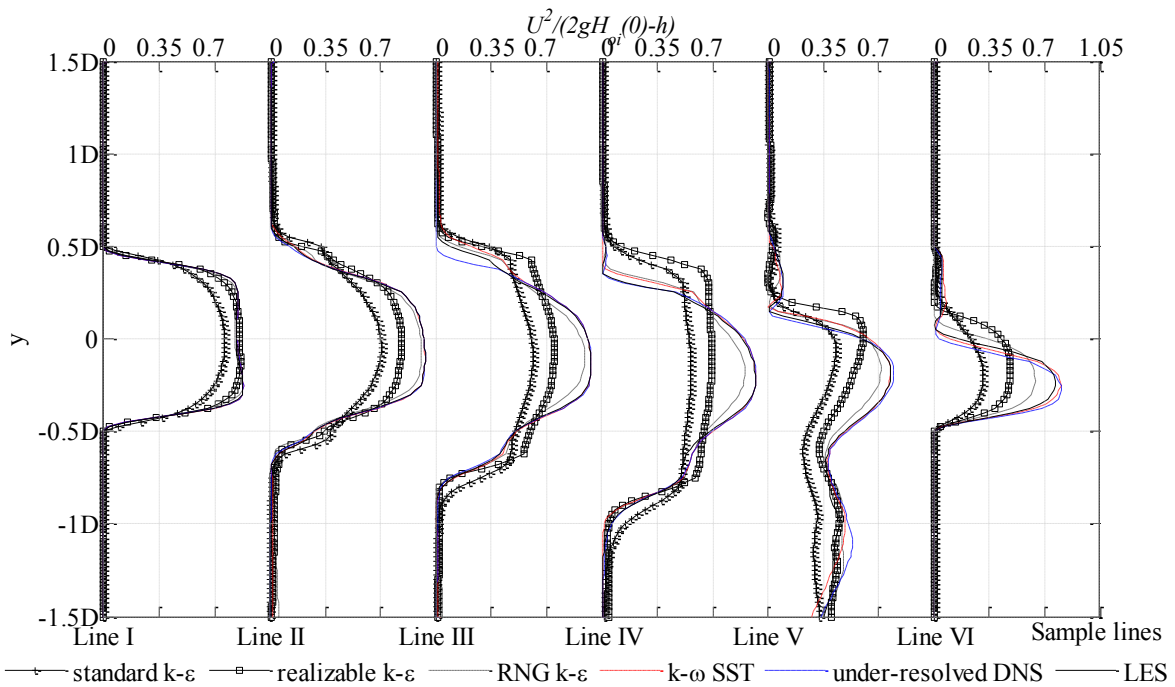

Figure 12   The profiles of the velocity head at different sampling lines in the central vertical plane with different at $t\sqrt{g/d} \approx 12$ for collision Case C1.
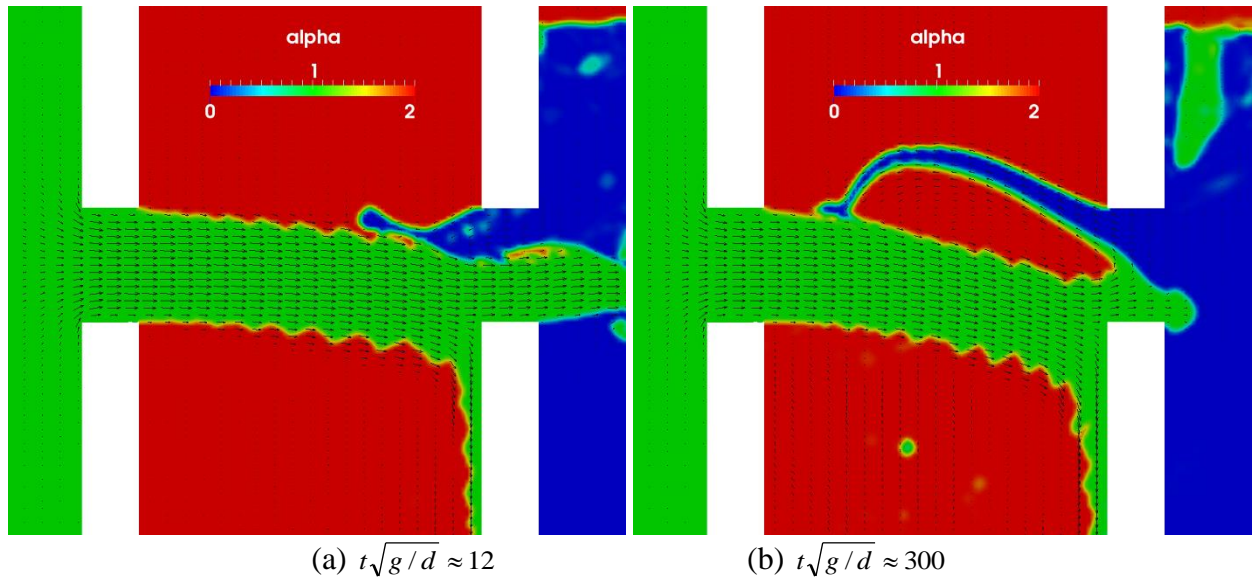
(a) $t\sqrt{g/d} \approx 12$ (b) $t\sqrt{g/d} \approx 300$

Figure 13 The velocity vector and distribution of the fluids at different time instants in Case C1 (LES modelling, the volume fraction, i.e. alpha, are 0, 1 and 2 for water, oil and air phase)
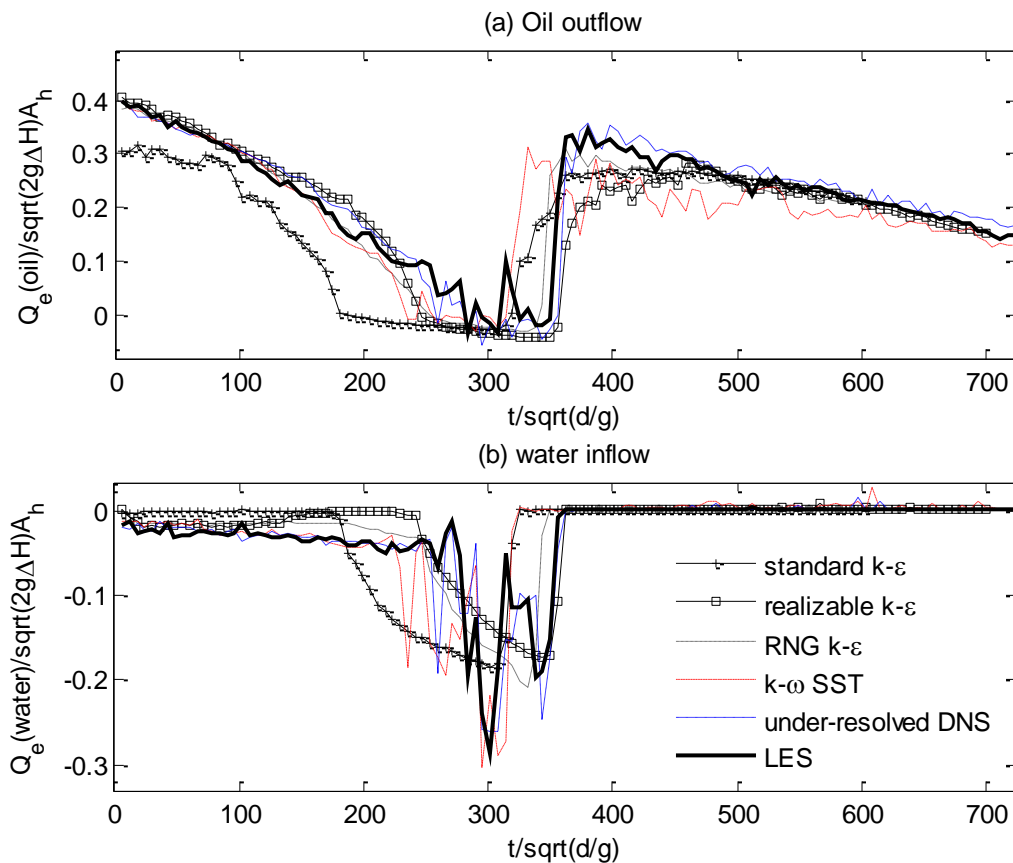

Figure 14 Time histories of discharges of the oil and water through the external hole in Case C1 (positive value means outflow)

A similar performance of the different turbulence modelling has also been observed in Case C1, as demonstrated in Fig. 12, which shows the profiles of velocity head at different locations at $t\sqrt{g/d} \approx 12$, though their features are very different from these in G1. For clarity, the velocity

vectors and the corresponding distribution of water, air and oil (represented by using the volume fraction) in the central vertical plane at the same time by using the LES modelling are illustrated in Fig. 13(a) for $t\sqrt{g/d} \approx 12$, which shows that water inflow from the environment and the oil outflow occur at the external hole simultaneously. It is also found from Fig. 13(b) that such convective motion of the oil outflow and the water inflow also occurs at other time instants. It is clearer in Fig. 14, which displays the time histories of discharges of the oil and water through the external hole in Case C1 (positive value of the discharge indicates an outflow). The instantaneous Reynolds number of the water inflow ($\tilde{V}_w 2\sqrt{\tilde{A}_w / \pi} / \gamma_w$ where γ_w is the kinematic viscosity of the water, $\tilde{V}_w$ and $\tilde{A}_w$ are the area-averaged water velocity and the cross-sectional area occupied by water) through the external hole may reach the level of 10^4 (Fig.15), which is much larger than the Reynolds number corresponding to the oil flow (i.e. ~1200) and indicates a typical turbulence regime. This implies that one may need to consider the Reynolds number corresponding to both the oil flow and the water inflow when classifying the significance of the turbulence and thus the suitability of the turbulence modelling.
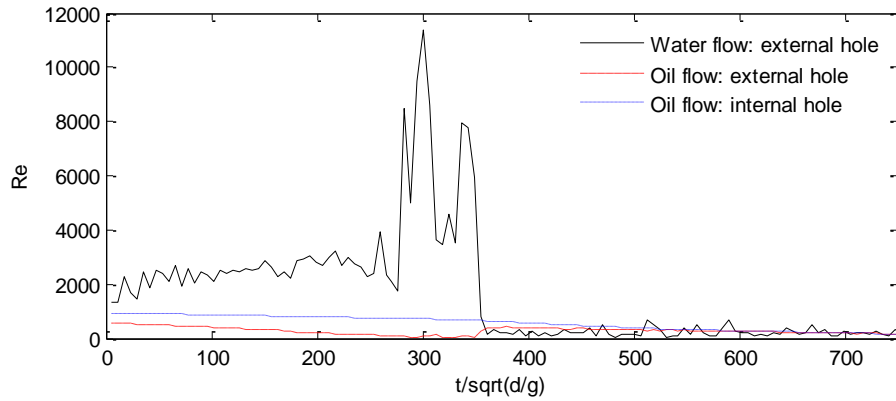

Figure 15 Instantaneous Reynolds numbers corresponding to the water and oil flow in Case C1 by using LES modelling(the instantaneous Reynolds number is obtained using $\tilde{V} 2\sqrt{\tilde{A}/\pi} / \gamma$ where γ is the kinematic viscosity, $\tilde{V}$ and $\tilde{A}$ are the areal averaged flow velocity and the cross-sectional area occupied by the fluid)
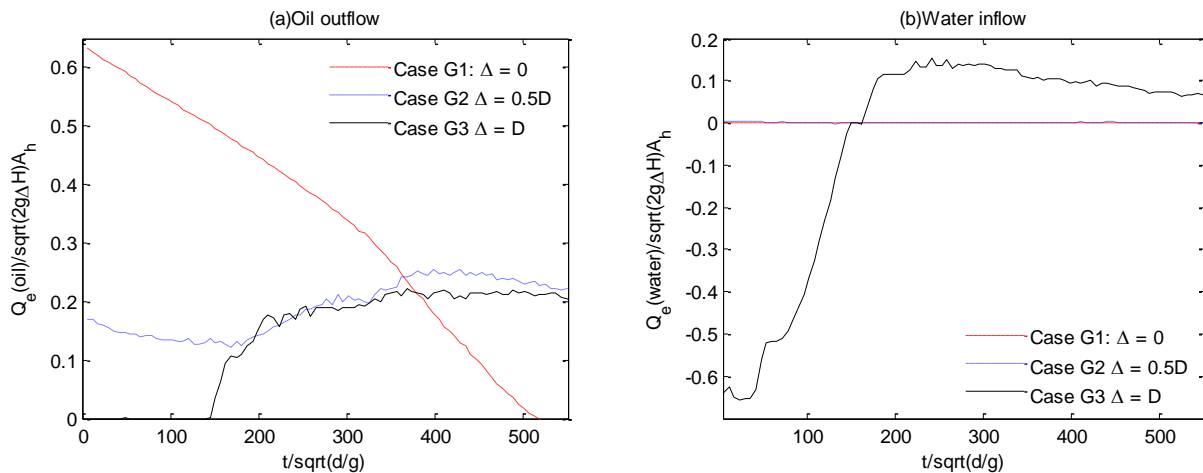

Figure 16 The comparison of the time histories of the discharges of the oil and water through the external hole in the cases with different axial offsets by LES modelling(D =2 cm, d = 27cm, initial H_{oil} = 42cm)

To do so, a group of cases with different offsets (Δ) between the internal and the external hole, i.e. G1, G2 and G3, are examined. As indicated above, different offsets (Δ) are expected to produce different characterised Re corresponding to the water inflow, whereas the characterised Re corresponding to the oil outflow remains approximately the same due to the same hydrostatic condition they applied. Fig. 16 plots the time histories of the discharges of the oil flow and the water flow through the external hole obtained using the LES modelling. One can see that discharges are significantly affected by the values of Δ. For example, in the case with Δ=0, no significant water inflow is detected but a considerable amount of water enter into the ballast tank from the beginning of the case with Δ=D. Another interesting point is that the water will be expelled out by oil in later stage in the case with Δ=D. As far as we know, such cases have not been investigated either numerically or experimentally so far in literature.

(a) $t\sqrt{g/d} \approx 0.16$　　　(b) $t\sqrt{g/d} \approx 0.19$　　　(c) $t\sqrt{g/d} \approx 0.57$
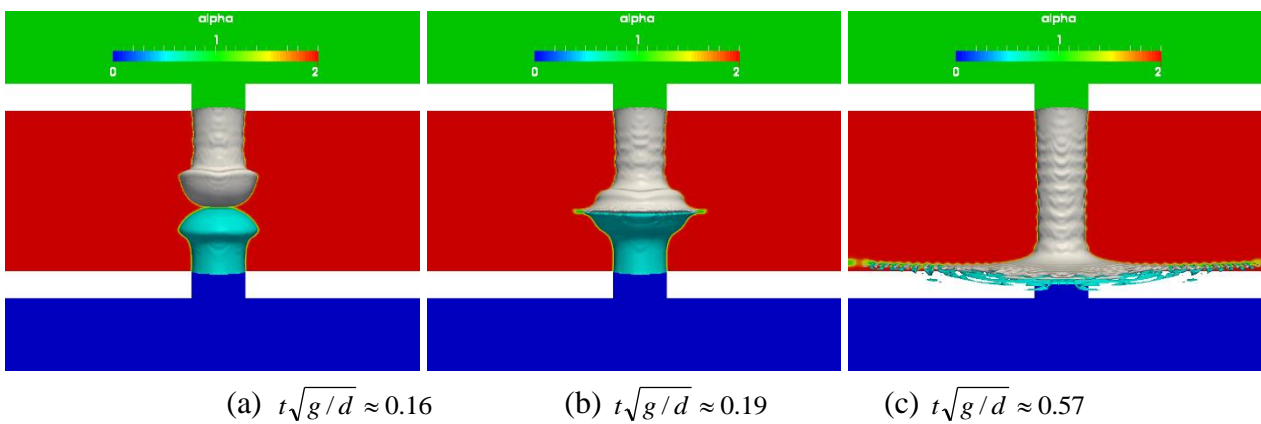
Figure 17 Snapshots of the oil jets in the ballast tank at different stages using the compressible LES simulation for Case G1 (the volume fraction, i.e. alpha, are 0, 1 and 2 for water, oil and air phase, the interfaces of the oil jet and water jet are marked by the grey and light blue iso-surfaces)
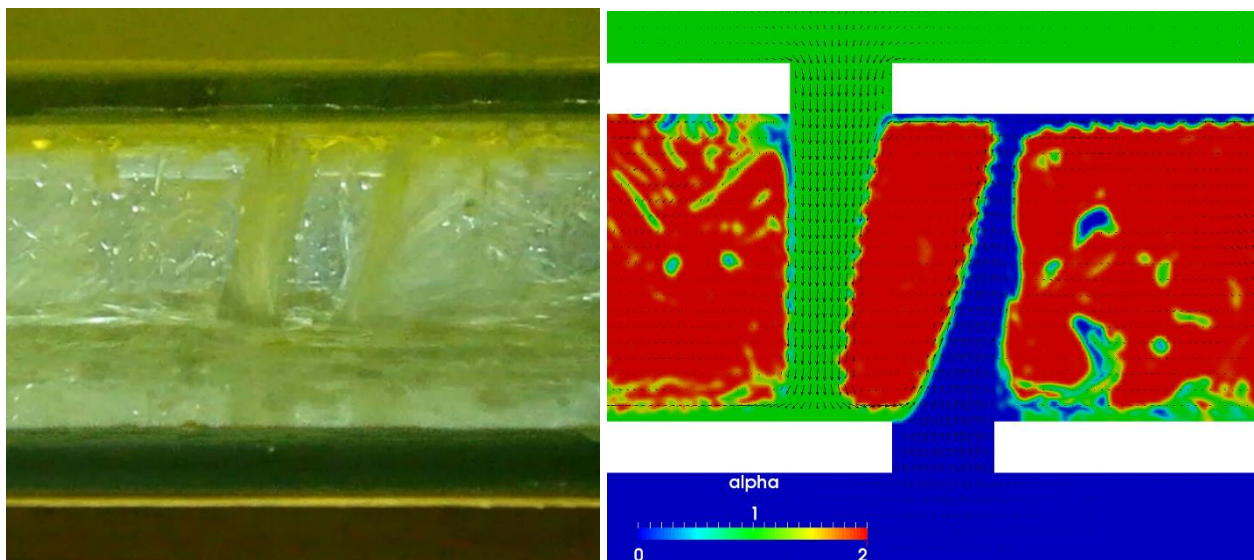
Figure 18 Flow pattern at $t\sqrt{g/d} \approx 12$ in Case G3 (Left: experimental data; Right: The velocity vector and distribution of the fluids in the central vertical plane in the LES modelling, the volume fraction, i.e. alpha, are 0, 1 and 2 for water, oil and air phase)

To explain why water inflow is not significant for the case with small offset, such as in Case G1 and Case G2, Fig. 17 is plotted for G1, in which one can see that the amount of water flow through

the external hole in the short period of the spilling from the start, e.g. $t\sqrt{g/d} < 0.5$. However, due to the strike of the downward oil jet from the internal tank, which carries higher momentum than the water jet, the upwelling water is pushed down. In Case G3, where the axial offset is D, such strike becomes insignificant and, therefore, in the early stage before the bottom ballast tanks becomes full ($t\sqrt{g/d} < 80$), the water inflow occupied the entire external hole and the downwards oil jets and the upwards water jets exist at the same time. It is clearer in Fig. 18 which compares the flow pattern obtained using the LES modelling and the experimental snapshot.
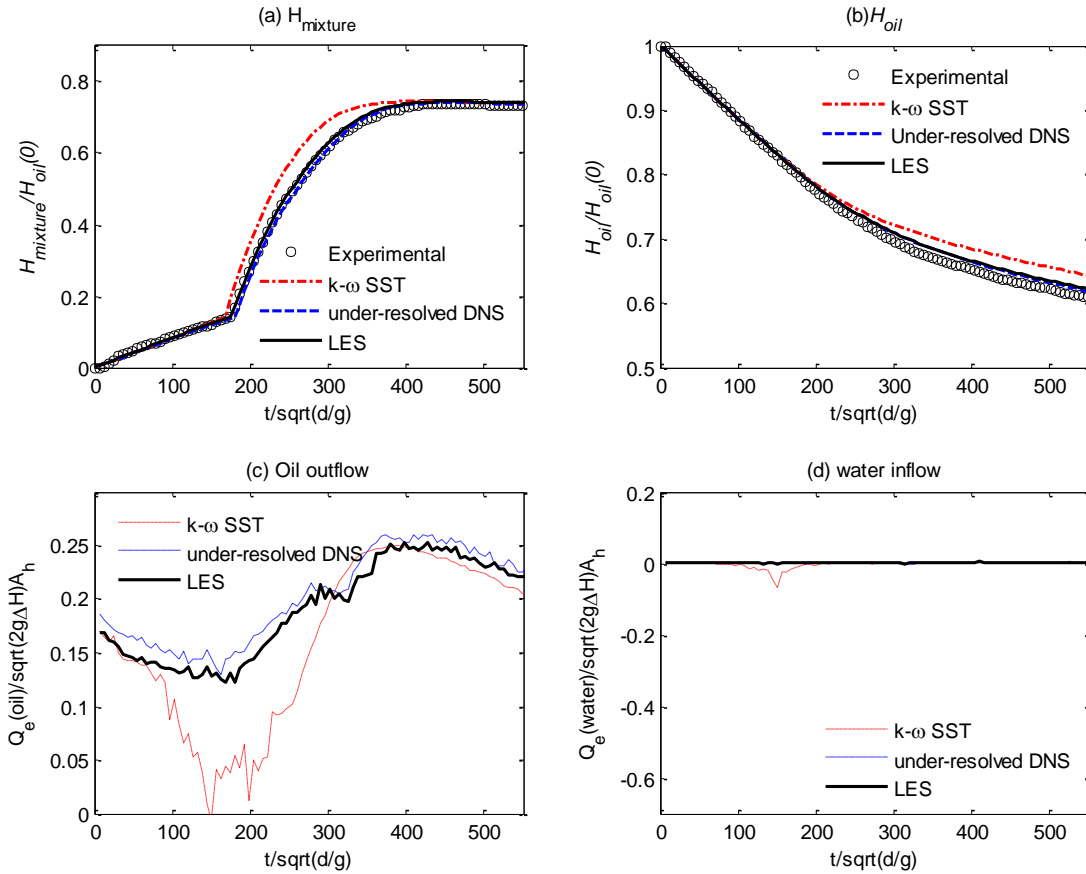

Figure 19 The comparison of the time histories of the mixture height in the ballast tank ($H_{mixture}$), the height of the oil in the cargo tank (H_{oil}), the discharges of the oil and water through the external hole in Case G2(D =2 cm, Δ = 1cm, d = 27cm, initial H_{oil} = 42cm)

The comparison of the time histories of the mixture height in the ballast tank ($H_{mixture}$), the height of the oil in the cargo tank (H_{oil}), the discharges of the oil and water through the external hole are shown in Fig. 19 and Fig. 20 for Case G2 with Δ = 1cm and Case G3 with Δ = 2cm, respectively. Only the results obtained by using the k-ω SST model, LES and the under-resolved DNS are given, considering relatively worse performance of the k-ε models in G1 and C1. Among the results, the H_{oil} and $H_{mixture}$ predicted by using the LES model agree well with the experimental data as in other two cases discussed in previous sections. The under-resolved DNS seems to be good as well, suggesting an insignificant contribution of the sub-grid tensors in these cases. However, the k-ω SST model performs worse in Case G2(Fig. 19) than in Case G1, showing a dramatic underestimation of the oil outflow and overestimation of the water inflow compared with the other

models. Compared with Case G1, the oil discharge from the internal tank in the Case G2 is at a similar level (Fig.6(b) and Fig.19(b)), whereas the oil outflow through the external hole in this case is less significant (Fig.19(c)). Fig.19(d) shows that the water inflow through the external hole is insignificant. Effectively, the Reynolds number indicating the turbulence in this case may be taken as that corresponding to the oil flow through the internal tank, i.e. ~1800, at the same level as that in Case G1. Nevertheless, the oil flow in Case G2 is more complex than that in Case G1 and shows more significant shearing behaviours due to the axial offset of the spilling hole. This implies that the importance of the transition turbulence near the interface between different phases relative to that associated with the jet flow through the broken holes may be greater in Case G2 than in Case G1. The k-ω SST model does not capture the free-shear layers correctly. It is also found that k-ω SST model produces numerical results close to the experimental data and the numerical results by other models in Case G3 (Fig. 20). In this case, during a long period from the start of the spilling until the level of the fluid in the ballast tank reaches a maximum value at $t\sqrt{g/d} \approx 150$, the external hole is only occupied by the water inflow with Reynolds number at the level of 4.6×10^{4}, greater than that in Case C1. The convective motion between the oil and water jets is less significant as demonstrated by Fig. 18, compared with those in Case C1 (Fig. 13). This means the importance of the transition turbulence associated with the free-shear layers (near the interfaces) relative to the turbulence associated with the jet flow through the broken hole in Case G3 is lower than that in Case C1.
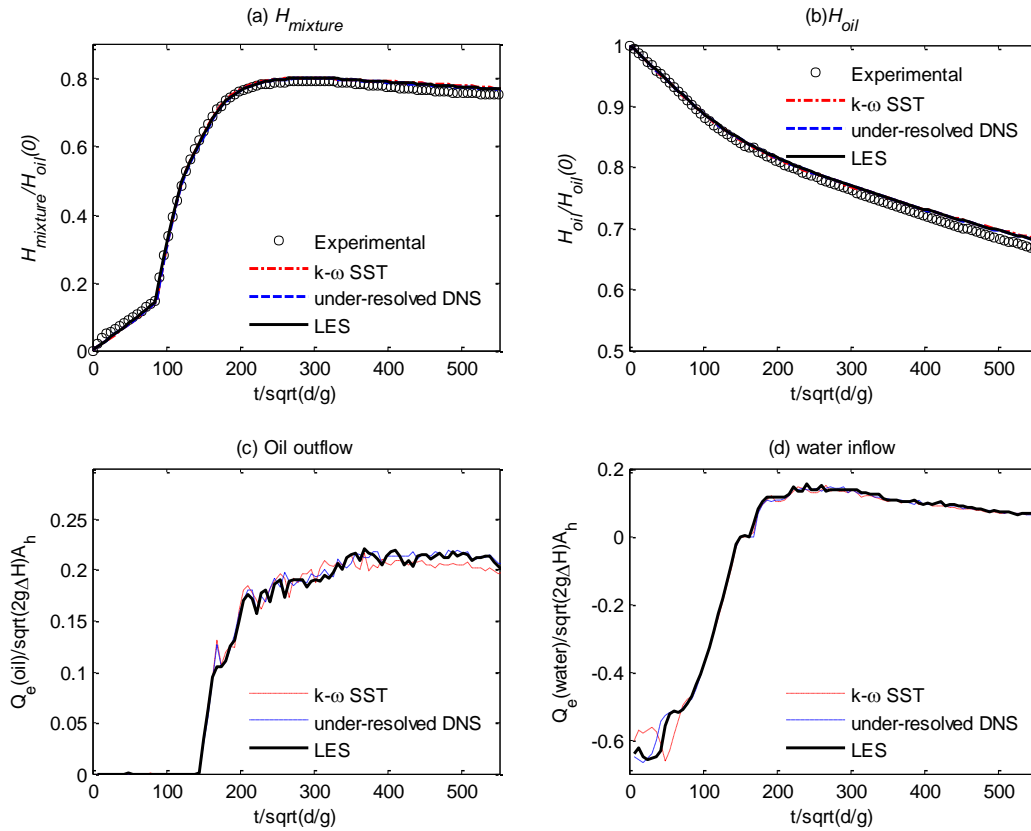

Figure 20 The comparison of the time histories of the mixture height in the ballast tank ($H_{mixture}$) and the height of the oil in the cargo tank (H_{oil}), the discharges of the oil and water through the external hole in Case G3(D =2 cm, $\varDelta$ = 2cm, d = 27cm, initial H_{oil} = 42cm)

From the above case studies, one may agree that both the turbulence associated with the jet flow through the broken hole and the transition turbulence near the interface between different phases associated with the oil spilling from a damaged DHT shall be considered. The significance of the former may be indicated by using the Reynolds number corresponding to the orifice flow. The latter is commonly classified by a sheared Reynolds number ([60, 61, 32]), which largely depends on the kinematics and the dynamics of the interface between different fluids and is not easy to be identified before the numerical simulations or laboratory experiments. For convenience, we use the former to classify the appropriate turbulence models for the oil spilling from DHTs in terms of computational robustness. Reynolds number corresponding to the water flow and to the oil flow shall be employed. Considering the fact that both the oil outflow and the water inflow are dominated by the gravity, we define the Reynolds numbers corresponding to the water flow and the oil flow, respectively, as $\mathrm{Re}_o = \dfrac{\sqrt{2g\Delta H_o}\, D}{\gamma_o}$ and $\mathrm{Re}_w = \dfrac{\sqrt{2g\Delta H_w}\, D}{\gamma_w}$ where subscripts 'o' and 'w' corresponds to the oil flow and water flow, respectively; ΔH_o is the initial potential head difference between the oil surface in the ballast tank and the internal hole; ΔH_w is the initial potential head difference between the external water surface and the external hole. These two Reynolds numbers may well indicate the turbulence associated with the water jet and oil jet detected in the early stage of the spilling (e.g. Fig. 17(a) for Case G1). Nevertheless, the water jet may not always significant, as shown in Fig. 17(c) where it disappears due to the strike with the oil jet that contains considerably larger momentum. Thus, the convective oil/water flow in the external hole becomes insignificant. For the cases where the significant water flow through the external hole is observed, e.g. Case C1 and Case G3, the effective Reynolds number for the classification is taken as $\max(\mathrm{Re}_o, \mathrm{Re}_w)$, otherwise, it is assigned to be Re_o.
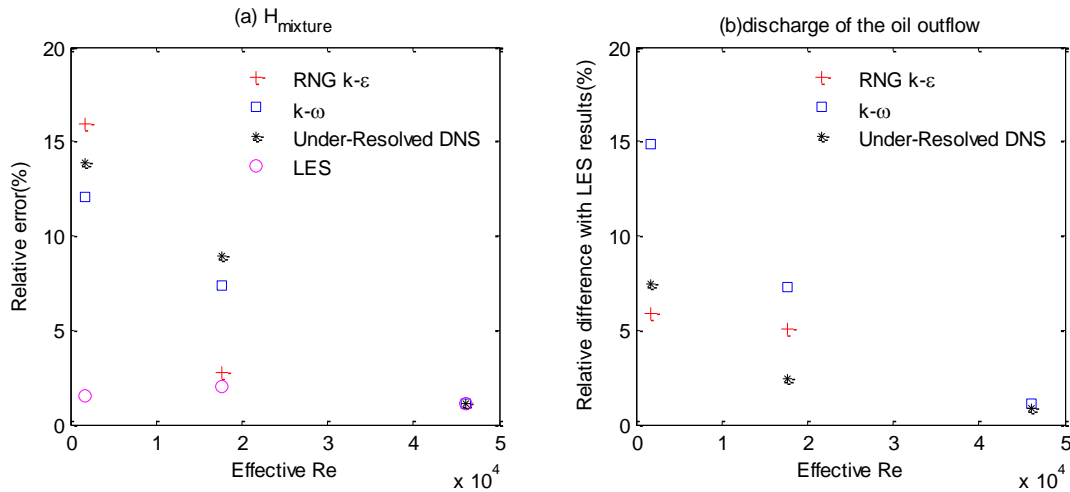
Figure 21 Relative errors in the cases with different turbulence models in terms of the effective Reynolds number

By using such definition of the effective Reynolds number, the comparison of relative errors in all cases considered in this paper is displayed in Fig. 21. The relative error in this figure is defined as $\int_t |f_n - f_e|\, dt \,/ \int_t |f_e|\, dt$ for parameter f to be considered; the subscript n represent the numerical results, and e represents the experimental data for $H_{mixture}$ in Fig. 21(a) but the LES results for discharge in

Fig. 21(b). For clarity, the corresponding results by the standard, low-Re and realizable k-ε models are not included due to their significantly larger errors compared to RNG k-ε and k-ω models, and only the corresponding maximum errors/difference are included in Fig.21. It is found that for a smaller effective Reynolds number, e.g. Case G1 and Case G2, the k-ε and k-ω SST lead to considerable large errors, though depending on which quantities are concerned with. For example, at effective Re $\sim 0.2 \times 10^4$, the relative errors of $H_{mixture}$ are 16% and 12% (Fig. 21a) for RNG k-ε and k-ω models, respectively, both much larger than the error (1.5%) of LES results; while the relative difference for discharge from the LES results are 6% and 15% (Fig. 21b) for RNG k-ε and k-ω models. If the errors at effective Re $\sim 1.8 \times 10^4$ are examined, one may found that the result of RNG k-ε model for $H_{mixture}$ is very close to that of LES (Fig. 21a) and the result of k-ω models is quite different from the LES results. However, if one examines Fig. 21b for discharge, one finds that the results from both models are significantly different from the LES results. Also observed from Fig.21, as the increase of the effective Reynolds numbers, the errors of RANS models trend to be reduced. For the high-Re case (i.e., Case G3 where effective Re $\sim 4.6 \times 10^4$), the k-ω model leads to the results that agree well with the experimental data and the results from LES in terms of both $H_{mixture}$ and discharge. It is also remarked that the agreement between the results by the under resolved DNS and the corresponding results by the LES becomes better as the increase of the effective Reynolds number. Considering the fact that they used the same mesh, this phenomenon implies that the effect of the sub-grid stress relative to the large eddy decreases as the increase of the effective Reynolds number. Based on the limited investigation in this paper, one may conclude that for low-Re cases with effective Reynolds number smaller than 18000, the LES shall be only used; whereas if the effective Reynolds number is greater than 40000, one may use the RANS approach, e.g. the k-ω SST , which generally requires less computational efforts compared to the LES. This also implies that the existing experiments ignoring the Reynolds similarity law for the water inflow may be not applicable to the cases with small Reynolds number of the oil flow. It should clarify that the 'low-Re' used in this conclusion is termed of the effective Reynolds number suggested above. In fact, in the low-Re cases, e.g. C1, the instantaneous Reynolds number may be high as demonstrated by Fig.15. Furthermore, in the present cases, the flow in the ballast tank does not only rely on the near-wall turbulence but also, perhaps more significantly, influenced by the turbulence associated with the interfaces between different liquid phases. This means that the low-Reynolds-number extensions of the commonly used RANS approaches (whose performance is improved mainly through imposing empirical functions near wall regions with fine grids, as a replacement of the wall function [55, 56]) may not be suitable for so-called low-Re cases here. This has been confirmed by our numerical results using Launder-Sharma low-Re k-ε model, as demonstrated in Figs. 6-8.

One may notice that such classification system depends on a reliable assessment on whether the water inflow through the external hole is significant. It is feasible to qualitatively address this issue through analysing the momentum brought by the water jet and the oil jet in the initial stage of the spilling. In the collision scenario with coaxial configurations (e.g. Case C1), the water inflow is usually considerable, because the self-weight of oil jets leads to a vertical fluid velocity component which leads to the situation that at the external hole, the oil jet does not cover the entire cross-sectional area. In the grounding scenario with coaxial configurations (e.g. Case G1), whether the water inflow is significant largely depends on whether the momentum brought by the upwards

water jets is more significant than that by the downwards oil jets (as shown in Fig. 17). Such hydrodynamic analysis on the behaviours of the oil/water jets are less relevant to the turbulence modelling discussed in this paper and therefore will be presented in our future publication to avoid defocusing the issues addressed in this paper.

4. ROLE OF COMPRESSIBILITY OF FLUIDS

As discussed in the previous Section, the entire process of the oil spilling includes several typical phenomena in which the compressibility may play an important role. The role of the compressibility of the fluids on the oil spilling from the damaged DHTs is discussed in this section. To do so, a compressible solver, in which the air phase is considered to be compressible, is used for all cases considered in this section. The results are compared with those achieved in the previous section using the incompressible solver. The LES model is employed in the compressible solver, considering the conclusion in Section 3. In the compressible solver, the equation of state for the ideal gas is adopted, where the gas coefficient (so does the speed of the sound) depends on the temperature fields obtained by the solutions of the thermodynamics with a heat capacity (C_v) for each phase translating the temperature into the internal energy ($C_{v(water)}$=4190J/kgK, $C_{v(air)}$=1005 J/kgK and $C_{v(oil)}$=1970J/kgK). The details of this model can be found in [62, 63]. The compressible solver has been validated by using a wide range of the experimental data available in literature, i.e. [64-66]. The convergence tests similar to that demonstrated in Section 2 are also carried out. The corresponding results will not be presented here to save the space.

We are aware that the compressibility of the fluids on the dynamics/kinematics of the fluids may be significant in a small spatial-temporal scale, e.g. during a short time of impact. To do so, the time histories of relevant dynamic and kinematic parameters are compared in a short duration near the occurrence of a violent fluid impact. Some results are shown in Fig.22 and Fig. 23 for demonstration. Fig. 22 compares the profiles (the front) of the oil jet at different time instants following the occurrence of its impact with the upwelling water jet as illustrated in Fig.17 at t=0.026s corresponds to the instant when the maximum pressure occurs (Fig. 23(b)). In this figure, z-axis origins from the exit of the internal hole.

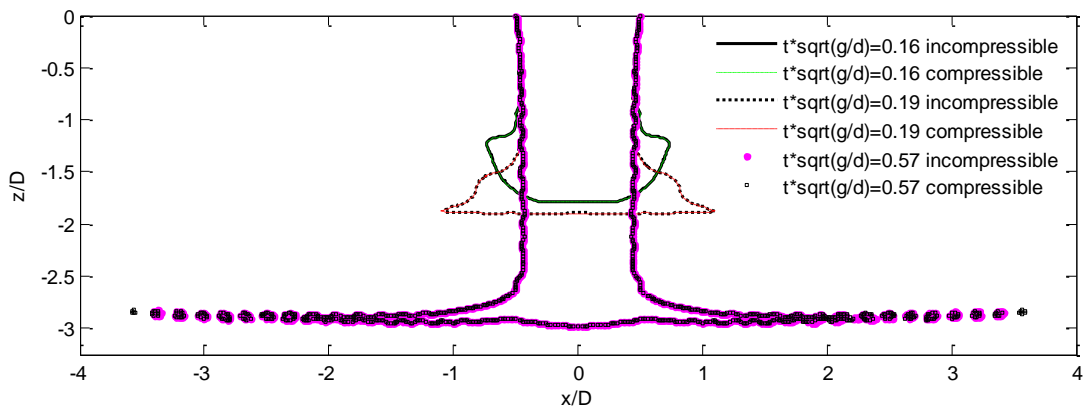Figure 22 Surface profiles of the oil jets at the central vertical plane in the transient stage of Case G1(z = -0.01m on the bottom surface of the internal hull)

It is found from Fig.22 that the profiles of the oil jet obtained using the incompressible solver agree well with the corresponding results by the compressible solver at $t\sqrt{g/d} \approx 0.16$ (Fig. 17(a)) and $t\sqrt{g/d} \approx 0.19$ (Fig.17(c)). At $t\sqrt{g/d} \approx 0.57$, when the main body of the oil jet reaches the external hole ($z/D = -3.0$), part of the oil jet hits the wall of the external hull and leads to oil splashing (Fig.17(c)). At this moment, the profile of the oil jet from the compressible solver largely agrees with that by the incompressible solver, except the shape of the splashing oil droplet. A further examinations of the location of the tip of the oil jet (at $x = 0$ in the central vertical plane) and its pressure are illustrated in Fig. 23. Again, a good agreement has been observed in terms of the location of the tip of the oil jet (Fig.23(a)) . However, from Fig. 23(b), where the pressure is normalised by the initial hydrostatic pressure at the internal hole, one may notice that the peak value of the pressure obtained by using the compressible solver ($1.884 \, \rho_{oil} g H_{oil}(0)$) is slightly higher than that by the incompressible solver ($1.805 \, \rho_{oil} g H_{oil}(0)$), although the overall time histories of the pressure by both solvers look very similar.
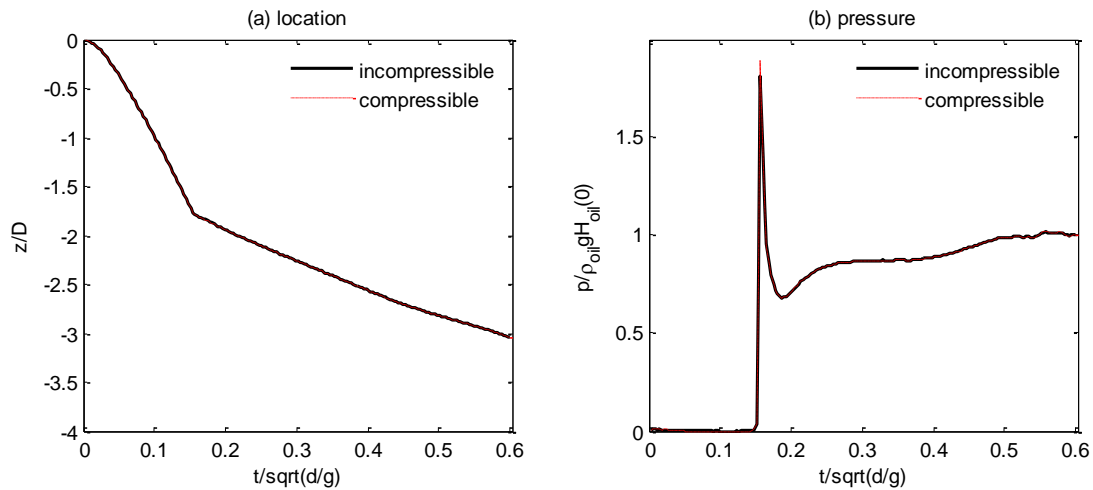

Figure 23 Time history of the location of the tip of the oil jet and the pressure on the tip in the transient stage of Case G1($z = -0.01$m on the bottom surface of the internal hull)

As the difference between the results by the compressible solver and the incompressible solver occurs in a very short duration, the role of compressibility of the fluid may be insignificant in a longer term. To examine how the compressibility of the fluids influences the macroscopic process of the oil spilling, the time histories of H_{oil} , $H_{mixture}$ and the discharge of the oil/water mixture through the internal(Q_i) and external (Q_e) holes are focused. Fig. 24 compares the corresponding results obtained by the compressible solver and the incompressible solver. For the purpose of comparison, the corresponding experimental data is also plotted together. For these macroscopic parameters, the results obtained by using the compressible and incompressible solvers are observed to be very close. Based on this observation, one may conclude that the compressibility of the fluid may only play a considerable role in a short duration of the impact and may be ignored in the numerical modelling of the oil spilling from damaged DHTs, especially if the macroscopic process is only focused.
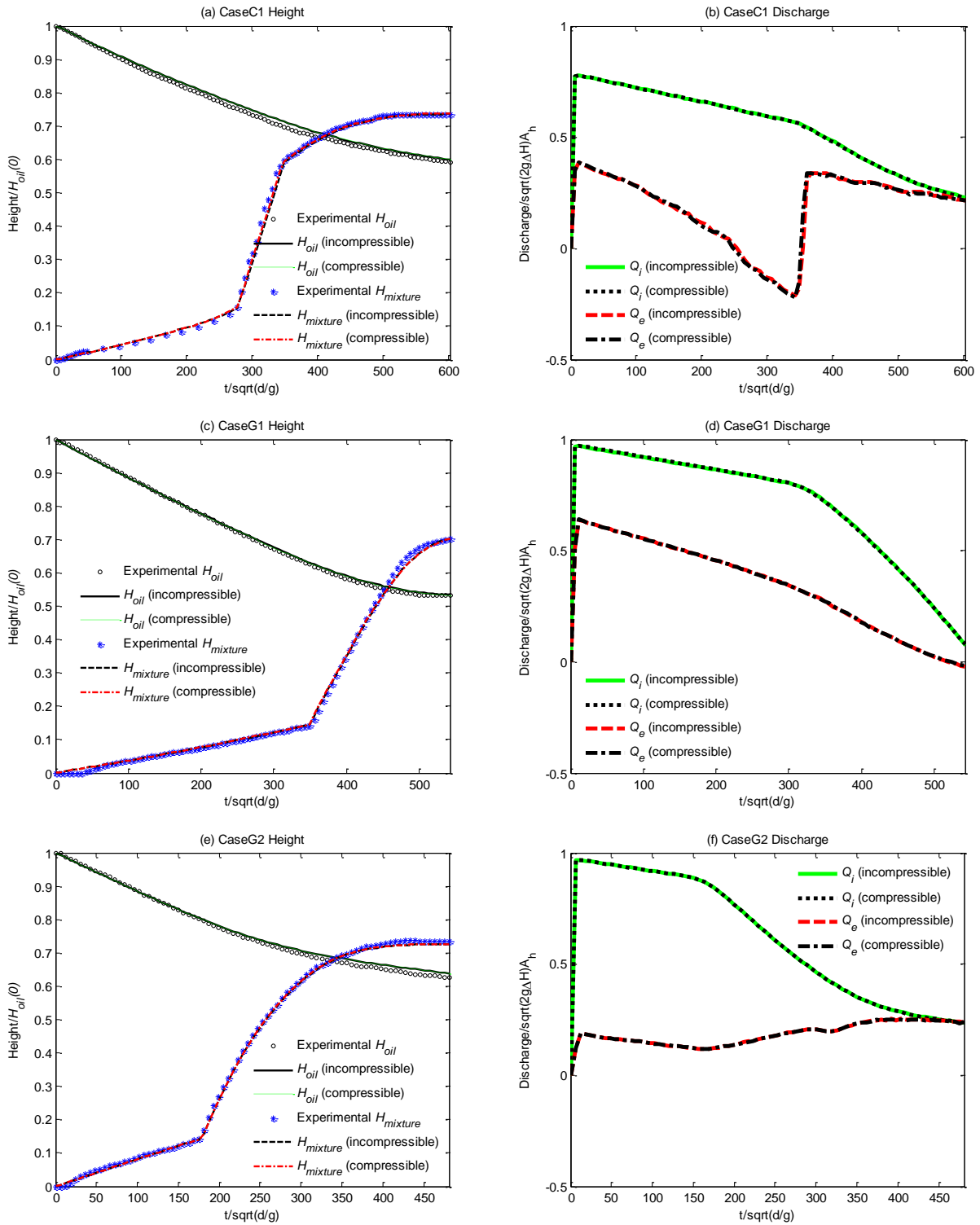
Figure 24 Time histories of the oil height in the cargo tank (H_{oil}) , the mixture height in the ballast tank ($H_{mixture}$) and the discharge of the mixture through the internal (Q_i) and external hole(Q_e) in the cases with or without considering the compressibility of the fluids

5. CONCLUSIONS

In this paper, both the experimental and numerical investigations have been carried out to look at the sensitivity of results to the turbulence modelling in order to give instructions to select an appropriate turbulence modelling approach to model the oil spilling from a damaged double hull

tanks (DHTs) and also at the role of the compressibility of the fluids, on oil spilling from a damaged double hull tanks (DHTs). In the experimental aspect, it is the first time to consider the effect of the axial offset of two holes in inner and outer hulls on the oil spilling from DHTs, to the best of our knowledge; both the grounding and collision scenarios have been considered. Such experiments lead to different characteristics of the water inflow whereas these of the oil outflow remain approximately the same, benefiting the development of a criterion to select the appropriate turbulence model. In the numerical aspect, various approaches to model the turbulence with both the compressible and incompressible solvers have been attempted. The results demonstrate the following conclusions. (1) The effective Reynolds number, considering not only the Reynolds number corresponding to the oil outflow but also that of the water inflow, must be employed when classifying the significance of the turbulence and selecting the appropriate turbulence model in terms of computational robustness. (2) At low effective Reynolds number, such as less than 18000, one should not use the RANS models as they do not yield sufficiently accurate results and one must choose the LES modelling. When effective Reynolds number is large enough, such as more than 40000, one may choose to use RANS models as they can give similar results to LES in terms of $H_{mixture}$ and discharge but costing much less CPU time. (3) Within the range of the applications studied in this paper, the significance of the sub-grid stresses relative to the large eddy decreases as the increase of the effective Reynolds number, consequently an under-resolved DNS may also lead to satisfactory results for $H_{mixture}$ and discharge in the cases with high effective Reynolds number; and (4) the compressibility of the fluids may play an important role in a short duration of the impact, leading to a considerable higher impact pressure, but does not significantly influence the macroscopic process of the oil spilling, for all cases considered in this paper.

These conclusions are reached from the cases considered in this paper. They need to be confirmed by a wider range of case studies. Nevertheless, the current knowledge about using the k-ε model for modelling the oil spilling from damaged tanks is now renewed by the findings in this paper.

ACKNOWLEDGMENTS

REFERENCES

1. Kim I. Ten years after the enactment of the Oil Pollution Act of 1990: a success or a failure. *Marine Policy* 2002; **26**:197-207.
2. Homan AC, Steiner T. OPA 90's impact at reducing oil spills. *Marine Policy* 2008; **32**:711-718.
3. Glen D. Modelling the impact of double hull technology on oil spill numbers, maritime policy & management. *The Flagship Journal of International Shipping and Port Research* 2010; **37**:475-487.
4. Yip TL, Talley WK, Jin D. The effectiveness of double hulls in reducing vessel-accident oil spillage. *Marine Pollution Bulletin* 2011; **62**:2427-2432.

5. Karafiath G. *Accidental oil spill due to grounding: summary of model test results*. NSWC: Bethesda, 1992.

6. Karafiath G, Bell RM. Model tests of accidental oil spill due to grounding. *Proceedings of the International Conference on Hydroscience and Engineering*, 1992.

7. Yamaguchi K, Yamanouchi H. Oil spills from the double hull model tanks. *The Report of Ship Technology Research Station* 1992; **29**:1-38.

8. Michel K, Moore C. Application of IMO's probabilistic oil outflow methodology. *SNAME Cybernautics '95 Symposium* 1995.

9. Rawson C, Crake K, Brown A. Assessing the environmental performance of tankers in accidental grounding and collision. *SNAME Transactions* 1998; **106**:41-58.

10. Smailys V, Česnauskis M. Estimation of expected cargo oil outflow from tanker involved in casualty. *Transport* 2006; **21**:293-300.

11. Van de Wiel G, Dorp JRV. An oil outflow model for tanker collisions and groundings. *Annals of Operations Research* 2009; **187**:279-304.

12. Goerlandt F, Montewka J. A probabilistic model for accidental cargo oil outflow from product tankers in a ship-ship collision. *Marine Pollution Bulletin* 2014; **79**:130-144.

13. Peter ACIII, Lin CW. Hydrodynamic analysis of oil outflow from double hull tankers. *Proceedings of the Advanced Double-Hull Technical Symposium* 1994.

14. Simecek-Beatty D, Lehr WJ, Lankford JE. Leaking tank experiments with Orimulsion^{TM} and Canola oil. *National Oceanic and Atmospheric Administration (NOAA) Technical Memorandum NOS OR&R* 6 2001; 1-30.

15. Lu JS, Gong XW, Yan SQ, Wen XF, Wu WQ. Experimental and numerical study on leakage of underwater hole on an oil tanker. *Proceedings of the 20th International Offshore and Polar Engineering Conference*, Beijing (China), 2010; 1047-1053.

16. Lu JS, Liu FC, Zhu ZY. Effects of initial water layer thickness on oil leakage from damaged DHTs. *Proceedings of the 24th International Offshore and Polar Engineering Conference*, Busan (South Korea), 2014; 618-623.

17. Tavakoli MT, Amdahl J, Leira BJ. Experimental investigation of oil leakage from damaged ships due to collision and grounding. *Ocean Engineering* 2011; **38**:1894-1907.

18. Tavakoli MT, Amdahl J, Ashrafian A, Leira BJ. Analytical predictions of oil spill from grounded cargo tankers. *Proceedings of the ASME 27th International Conference on Offshore Mechanics and Arctic Engineering*, Estoril (Portugal), 2008; 911-920.

19. Tavakoli MT, Amdahl J, Leira BJ. Investigation of interaction between oil spills and hydrostatic changes. *Proceedings of the ASME 28th International Conference on Offshore Mechanics and Arctic Engineering*, Hawaii (USA), 2009; 803-811.

20. Tavakoli MT, Amdahl J, Leira BJ. Analytical and numerical modelling of oil spill from a side tank with collision damage. *Ship and Offshore Structures* 2012; **7**:73-86.

21. Sergejeva M, Laanearu J, Tabri K. Hydraulic modelling of submerged oil spill including tanker hydrostatic overpressure. *Analysis and Design of Marine Structures* 2013; 209-217.

22. Yang H, Lu JS, Yan SQ. Preliminary numerical study on oil spilling from a DHT. *Proceedings of the 24th International Ocean and Polar Engineering Conference*, Busan (Korea), 2014; 610-617.

23. Xiao M, Li W, Lin JG, Liang X. Numerical simulation of oil spill trajectory and velocity for wrecked ship. *Journal of Dalian Maritime University* 2010; **36**:121-124.

24. Krata P, Jachowski J, Montewka J. Modeling of accidental bunker oil spills as a result of ship's bunker tanks rupture - a case study. *The International Journal on Marine Navigation and Safety of Sea Transportation* 2012; **6**:495-500.

25. Koshizuka S, Oka Y. Moving-particle semi-implicit method for fragmentation of incompressible fluid. *Nuclear Science and Engineering* 1996; **123**:421-434.

26. Cheng LY, Gomes DV, Nishimoto K. A numerical study on oil leakage and damaged stability of oil carrier. *Proceedings of the ASME 2010 29th International Conference on Ocean, Offshore and Arctic Engineering*, Shanghai (China), 2010; 829-836.

27. Lee BH, Park JC, Kim MH, Hwang SC. Step-by-step improvement of MPS method in simulating violent free-surface motions and impact loads. *Computer Methods in Applied Mechanics and Engineering* 2011; **200**:1113-1125.

28. Dabiri S, Sirignano WA, Joseph DD. Cavitation in an orifice flow. *Physics of Fluids* 2007; **19**: 072112.

29. Arun N, Malavarayan S, Kaushik M. CFD analysis on discharge coefficient during non-Newtonian flows through orifice meter. *International Journal of Engineering Science and Technology* 2010; **2**:3151-3164.

30. Hollingshead CL, Johnson MC, Barfuss, SL, Spall, RE. Discharge coefficient performance of Venturi, standard concentric orifice plate, V-cone and wedge flow meters at low Reynolds numbers. *Journal of Petroleum Science and Engineering* 2011; **78**:559-566.

31. Hunt CR, Eames I, Westerweel J. Mechanics of inhomogeneous turbulence and interfacial layers. *Journal of Fluid Mechanics* 2006; **554**:499-519.

32. Reboux S, Sagaut P, Lakehal D. Large-eddy simulation of sheared interfacial flow. *Physics of Fluids* 2006; **18**:105-105.

33. Pan Y, Suga K. A numerical study on the breakup process of laminar liquid jets. *Physics of Fluids* 2006; **18**:052101-1.

34. Zhang QD, Tan CS, Sundaravadivelu K. Mitigation of flow induced vibration of head gimbal assembly. *Microsystem Technology: Sensors, Actuators, Systems Integration* 2010; **16**:213-219.

35. Salim SM, Buccolieri R, Chan A, Sabatino SD. Numerical simulation of atmospheric pollutant dispersion in an urban canyon: comparison between RANS and LES. *Journal of Wind Engineering and Industrial Aerodynamics* 2011; **99**:103-113.

36. Ma ZH, Causon DM, Qian L, Mingham CG, Gu HB, Ferrer PM. A compressible multiphase flow model for violent aerated wave impact problem. *Proceedings of the Royal Society A* 2014; **470**: 20140542.

37. Lind S, Stansby P, Rogers B, Lloyd P. Numerical predictions of water-air wave slam using incompressible-compressible smoothed particle hydrodynamics. *Applied Ocean Research* 2015; **49**:57-71.

38. Papanikolaou A, Zaraphonitis G, Boulougouris E, Langbecker U, Matho S, Sames P. Multi-objective optimization of oil tanker design. *Journal of Marine Science and Technology* 2010; **15**:359-373.

39. Udeagbara SG. *Effect of temperature and impurities on surface tension of crude oil*. Dissertation.com: Boca Raton (USA), 2009.

40. Weller HG. *A new approach to VOF-based interface capturing methods for incompressible and compressible flow*. OpenCFD Ltd: Bracknell (UK), 2008.

41. Flingoh CHOH, Chong CL. Surface tensions of palm oil, palm olein and palm stearin. *ELAEIS* 1992; **4**:27-31.

42. Dean JA. *Lange's handbook of chemistry*. McGraw-Hill: London, 1999.

43. Konno A, Izumiyama K. On the relationship of the oil/water interfacial tension and the spread of oil slick under ice cover. *Proceedings of the 17th International Symposium on Okhotsk Sea and Sea Ice*, 2002; 275-282.

44. McNaught JM. *Methods for effective viscosity of two immiscible liquid phases*. AspenTech: Houston (USA), 2011.

45. Gebreslassie MG, Tabor GR, Belmont MR. Numerical simulation of a new type of cross flow tidal turbine using OpenFOAM – Part I: calibration of energy extraction. *Renewable Energy* 2013; **50**:994-1004.

46. Gourdain N. Prediction of the unsteady turbulent flow in an axial compressor stage. Part 1: Comparison of unsteady RANS and LES with experiments. *Computers & Fluids* 2015; **106**:119-129.

47. Taghinia J, Rahamn MM, Siikonen T, Agarwal RK. One-equation sub-grid scale model with variable eddy-viscosity coefficient. *Computers & Fluid* 2015; **107**:155-164.

48. Menon S, Yeung PK, Kim WW. Effect of subgrid models on the computed interscale energy transfer in isotropic turbulence. *Computers & Fluids* 1996; **2**:165-180.

49. Stringer R, Zang J, Hillis AJ. Unsteady RANS computations of flow around a circular cylinder for a wide range of Reynolds numbers. *Ocean Engineering* 2014; **87**:1-9.

50. Yan SQ, Ma QW. Numerical simulation of interaction between wind and 2D freak waves. *European Journal of Mechanics B/Fluids* 2010; **29**:18-31.

51. Wardle KE. Open-source CFD simulations of liquid-liquid flow in the annular centrifugal contactor. *Separation Science and Technology* 2011; **46**:2409-2417.

52. Ma QW, Yan SQ. Quasi ALE finite element method for nonlinear water waves. *Journal of Computational Physics* 2006; **212**:52-72.

53. Ramya BN, Yogesh KKJ, Seshadri V. Numerical analysis of the performance characteristics of conical entrance orifice meter. *International Journal of Engineering Sciences & Research Technology* 2015; **4**:209-217.

54. Liu HF, Tian H, Chen H, Jin T, Tang K. Numerical study on performance of perforated plate applied to cryogenic fluid flowmeter. *Journal of Zhejiang University SCIENCE A* 2015; In press.

55. Seyedein SH, Hasan M, Mujumdar AS. Modelling of a single confined turbulent slot jet impingement using various k-ε turbulence models. *Applied Mathematical Modelling* 1994; **10**: 526-537.

56. Cho HH, Goldstein RJ. An improved low-Reynolds-number k-ε turbulence model for recirculating flows. *International Journal of Heat and Mass Transfer* 1994; **37**:1495-1508.

57. Höhne T, Mehlhoop JP. Validation of closure models for interfacial drag and turbulence in numerical simulations of horizontal stratified gas-liquid flows. *International Journal of Multiphase flow* 2014; **62**:1-16.

58. Karim MM, Rahman MM, Alim MA. Computation of Axisymmetric turbulent viscous flow around sphere. *Journal of Scientific Research* 2009; **1**:209-219.

59. El-Behery SM, Hamed MH. A comparative study of turbulence models performance for separating flow in a planar asymmetric diffuser, *Computers & Fluids* 2011; **44**:248-257.

60. Lombardi P, Angelis VD, Banerjee S. Direct numerical simulation of near-interface turbulence in coupled gas-liquid flow. *Physics of Flui*ds 1996; **8**:1643-1665.

61. Fulgosi M, Lakehal D, Banergee S, Angelis VD. Direct numerical simulation of turbulence in a sheared air-water flow with a deformable interface. *Journal of Fluid Mechanics* 2003; **482**:319-345.

62. Miloshevsky G, Hassanein A. Splashing and boiling mechanisms of melt layer losses of PFCs during plasma instabilities. *Journal of Nuclear Materials* 2013; **438**:S155:S159.

63. Calderón-Sánchez J, Duque D, Gómez-Goñi J. Modeling the impact pressure of a free falling liquid block with OpenFOAM. *Ocean Engineering* 2015; **103**:144:152.

64. French JA. Wave uplift pressure on horizontal platforms. *Report No. KH_R_19, W.M. Keck Laboratory of Hydraulics and Water Resources*, California Institution of Technology, Pasadena, California, 1969.

65. Hu CH, Kashiwagi M. A CIP-based method for numerical simulations of violent free-surface flows. *Journal of Marine Science and Technology* 2004; **9**:143-157.

66. Ma ZH, Qian L, Causon DM, Mingham CG, Mai T, Greaves D, Raby A. The role of fluid compressibility in predicting slamming loads during water entry of flat plates. *Proceedings of the 25th International Offshore and Polar Engineering Conference*, Hawaii (USA), 2015; 642-646.